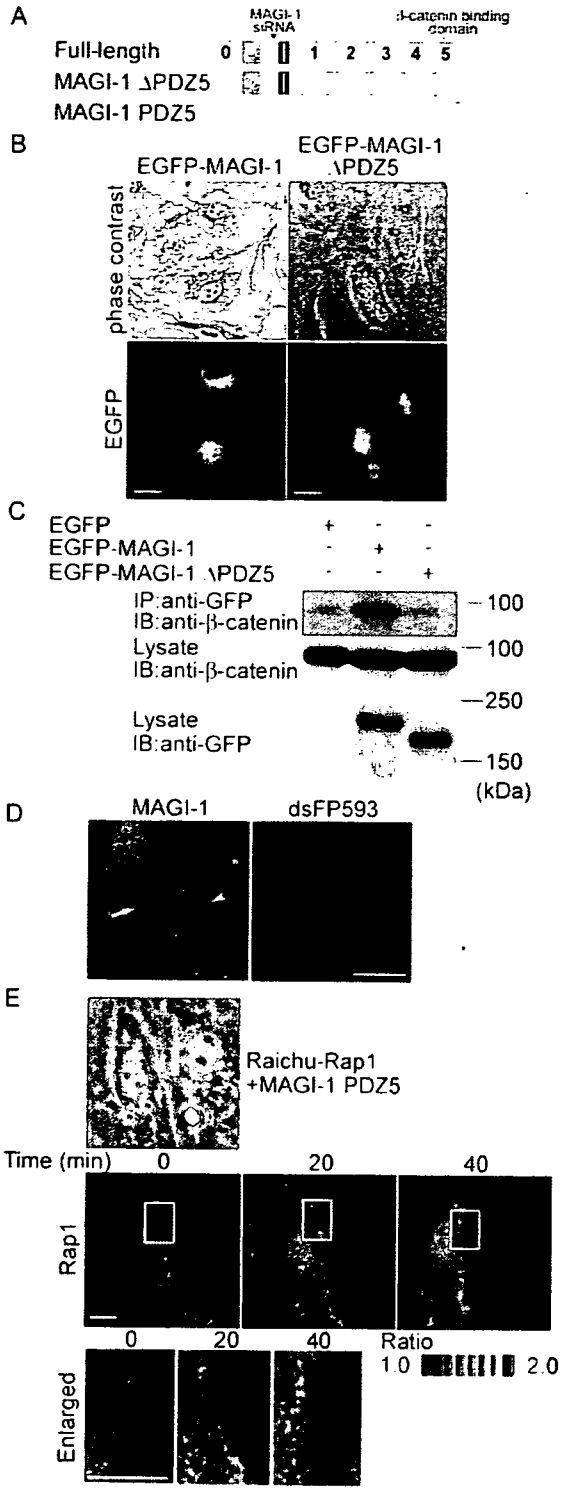

Figure 4. MAGI-1 localizing to cell–cell contact via β-catenin is required for Rap1 activation. (A) Schematic illustration of MAGI-1 and its mutants. The corresponding region of siRNA for MAGI-1 used in Figure 5 is also indicated in this schema.(B) HUVECs were transfected with the plasmids indicated at the top and imaged on an Olympus IX-81 fluorescent microscope. Bars, 20 μm. Note the localization of EGFP-MAGI-1 at the cell–cell contact but not MAGI-1 lacking PDZ domain 5. (C) 293T cells were transfected with the plasmids as indicated at the top. Cell lysates were subjected to immunoprecipitation (IP) with anti-GFP followed by immunoblotting (IB) or directly to immunoblotting using the antibodies indicated at the left. Note that endogenous β-catenin is coimmunoprecipitated with EGFP-tagged MAGI-1, but not with that lacking PDZ5. (D) HUVECs expressing PDZ domain 5 of MAGI-1 was immunostained with anti-MAGI-1 antibody. No immunoreaction was detected at the cell–cell contact between PDZ domain 5-expressing cells (arrow), whereas immunoreaction was detected at the contact between PDZ domain 5-expressing cell and untransfected cell (arrow-head). (E) HUVECs transfected with Raichu-Rap1 and pIRM21-MAGI-1–PDZ5 were FRET-imaged (middle). Phase contrast image was overlaid onto the image for dsFP593 to distinguish HUVECs transfected with pIRM21-MAGI-1–PDZ5 from those transfected only with Raichu-Rap1 (top). Red and blue hues indicated by intensity modulated display reflect increased and decreased FRET, respectively. The boxed regions in the middle panels were enlarged (bottom). The upper and lower limits of the ratio range are shown at the bottom right. Bars, 20 μm.

was almost completely reduced, as examined by Western blotting (Figure 5A). MAGI-1 at the cell–cell junction was not found in the cells treated with siRNA, as examined by immunostaining (Figure 5B). In the same setting, siRNA-introduced HUVECs expressing Raichu-Rap1 were subjected to FRET imaging. Rap1 activation upon cell–cell contact was significantly suppressed in MAGI-1-depleted cells (Figure 5C and Supplementary Movie 5). Quantitative FRET imaging analysis was performed to quantitatively analyze the activation of Rap1 at the cell–cell contacts in MAGI-1-depleted cells (Figure 5D and Supplementary Figure 2). We notice that Rap1 activation was detected at the free ruffled membrane without cell–cell contacts, similarly to control cells (Supplementary Movies 1 and 5), even in the MAGI-1-depleted cells. Collectively, these data suggest that the localization of MAGI-1 to cell–cell contacts through binding to β-catenin is involved in Rap1 activation.

Depletion of MAGI-1 Results in Impairment of VE-Cadherin-based Cell Adhesion

To elucidate the role of activated Rap1 downstream of MAGI-1 upon cell–cell contact, we examined the effect of depletion of MAGI-1 on VE-cadherin/β-catenin-based cell–cell contact after calcium switch. The localization of VE-cadherin and β-catenin at cell–cell contacts in confluent monolayer-cultured HUVECs was unchanged by MAGI-1 siRNA treatment. Because calcium switch induces cadherin-mediated cell junction after its disruption, we looked at the localization of VE-cadherin and β-catenin during calcium switch by immunostaining for VE-cadherin and β-catenin. VE-cadherin was reaccumulated at cell–cell junctions together with β-catenin within 20 min in control HUVECs. In clear contrast, there was a significant impairment of the formation of VE-cadherin/β-catenin-based cell junction in MAGI-1-depleted HUVECs (Figure 6).

TJ formation was not affected by MAGI-1 depletion and calcium switch (Figure 7A), whereas the recovery of VE-cadherin-based cell adhesion was substantially impaired in MAGI-1-depleted cells. These results indicate that MAGI-1-mediated signal is important for VE-cadherin/β-catenin-based cell adhesion.

We and others have previously reported that Rap1 activation enhances cell adhesions (Fukuhara *et al.*, 2005; Kooistra *et al.*, 2005). Cortical actin formation is enhanced by Rap1 activation and strengthens VE-cadherin-based cell–cell adhesion. Vinculin supports the cortical actin by linking α-catenin to α-actinin and by directly functioning as an

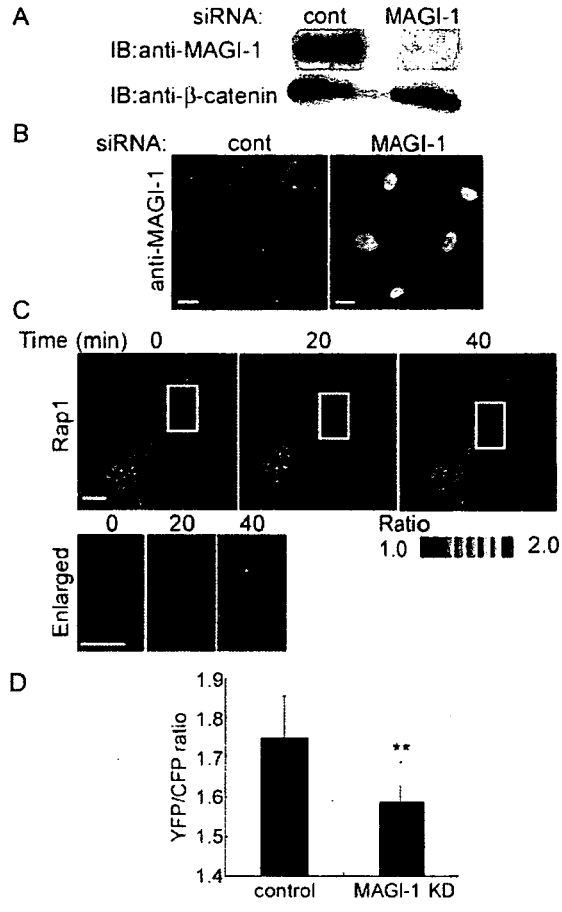

Figure 5. Depletion of MAGI-1 inhibits Rap1 activation upon cell–cell contact. (A) HUVECs transfected with control siRNAs or MAGI-1 siRNAs were cultured for 48 h. The cells were lysed, subjected to SDS-PAGE, and immunoblotted with anti-MAGI-1 and anti-β-catenin. (B) HUVECs transfected with control siRNAs or MAGI-1 siRNAs were cultured for 48 h and immunostained with anti-MAGI-1. Bars, 20 μm. (C) MAGI-1-depleted HUVECs were infected with Adeno-Raichu-Rap1 and FRET-imaged. The ratio-images indicate Rap1 activation by red hue and Rap1 inactivation by blue hue (top). The boxed region between two neighboring cells is enlarged (bottom). Bars, 20 μm. (D) Quantitative FRET analysis at the cell–cell contacts were performed in cells treated with control siRNA-treated HUVECs (control) and with MAGI-1-depleted cells (MAGI-1 KD). Quantitative FRET analysis is explained in Supplementary Figure 2. Mean values with standard deviations obtained by 30 cell–cell contact sites are shown as a representative result of three independent experiments. Statistical significance was analyzed by Student's *t* test and is indicated as ** $p < 0.01$.

actin-bundling molecule (Kobielak and Fuchs, 2004). Thus we investigated the vinculin localization after calcium switch by immunostaining. Vinculin was observed at the cell-ECM contacts presumably by translocating from cell–cell contacts after calcium depletion. Calcium restoration induced the relocation of vinculin from cell-ECM to cell–cell contact in control siRNA-treated cells. In clear contrast, vinculin remained at the focal adhesions in MAGI-1-depleted cells after calcium switch (Figure 7B). These data suggest that MAGI-1-dependent Rap1 activation at cell–cell contact may affect the vinculin localization, thereby regulating VE-cadherin-based cell adhesion.

MAGI-1 Is Required for VE-Cadherin-mediated Cell Adhesion

Vascular endothelial cell adhesion entails VE-cadherin-based adhesion and other cell adhesion molecules-based cell adhesion. To directly assess the involvement of MAGI-1 in VE-cadherin-mediated cell adhesion, we examined the adhesion of control siRNA-treated HUVECs and MAGI-1-depleted HUVECs onto VEC-Fc-coated dishes. The adhesion was quantified by the ALP activity of cells attaching to the dish after washing. Control HUVECs adhered to the VEC-Fc-coated dish in a time-dependent manner, whereas MAGI-1-depleted HUVECs exhibited significantly impaired adhesion to the VEC-Fc-coated dish (Figure 8A). No cells attached to the Fc-coated dish. MAGI-1-depleted HUVECs adhered to the collagen-coated dish comparably to control HUVECs (Figure 8B). We proceeded to examine the effect of inactivation of Rap1 on VE-cadherin-dependent adhesion. Control adenovirus-infected HUVECs adhered to VEC-Fc-coated dish, whereas Rap1GAPII-expressing adenovirus-infected HUVECs did not (Figure 8C). These results indicate that MAGI-1 and Rap1 activation is required for VE-cadherin-dependent cell adhesion.

DISCUSSION

FRET imaging enabled us for the first time to show the activation of Rap1 at the endothelial cell–cell junction, although previously Rap1 was suggested to be activated upon cell adhesion. In epithelial cells, C3G associating with E-cadherin is responsible for Rap1 activation upon cell contacts (Hogan *et al.*, 2004). Rap1, vice versa, regulates E-cadherin-mediated cell adhesion (Price *et al.*, 2004). In addition to E-cadherin, homophilic dimerization of nectin at the AJs triggers Rap1 activation downstream of Src-Crk (Fukuyama *et al.*, 2005). During the calcium switch experiment, which requires extracellular Ca^{2+}, we found that Rap1 was activated (Figure 1C), indicating extracellular Ca^{2+}-dependent signal, namely cadherin- and nectin-independent signal, appears to be involved in Rap1 activation upon cell–cell contact. In the present study, we propose the involvement of the MAGI-1/PDZ-GEF1 complex in Rap1 activation, besides nectin-mediated Rap1 activating signal and the subsequent positive feedback regulation of VE-cadherin-mediated cell adhesion.

Rap1 is responsible for maintenance and maturation of AJs. The establishment of cadherin-dependent cell–cell contacts is attributable to Rap1 in *Drosophila melanogaster* and mammalian cells (Knox and Brown, 2002; Price *et al.*, 2004). Consistently, we show here that VE-cadherin-dependent cell adhesion triggers a signal implicating MAGI-1 in Rap1 activation, presumably the MAGI-1–PDZ-GEF1-Rap1 pathway. VE-cadherin engagement-induced Rap1 activation may contribute to AJ formation in addition to homophilic engagement of nectin-dependent Rap1 activation (Fukuyama *et al.*, 2005).

Here we demonstrate VE-cadherin-dependent Rap1 activation besides nectin-dependent Rap1 activation. Calcium switch does not alter localization of nectin at the cell–cell contacts (Yamada *et al.*, 2005). We found that Rap1 was activated after calcium restoration in the calcium switch experiment that mimics nascent cell–cell contact formation (Figure 1), indicating that Ca^{2+}-dependent cell–cell contact is involved in Rap1 activation. We first assumed that VE-cadherin is responsible for Rap1 activation. Indeed, VE-cadherin depletion inhibited cell–cell contact-mediated Rap1 activation (Figure 1F).

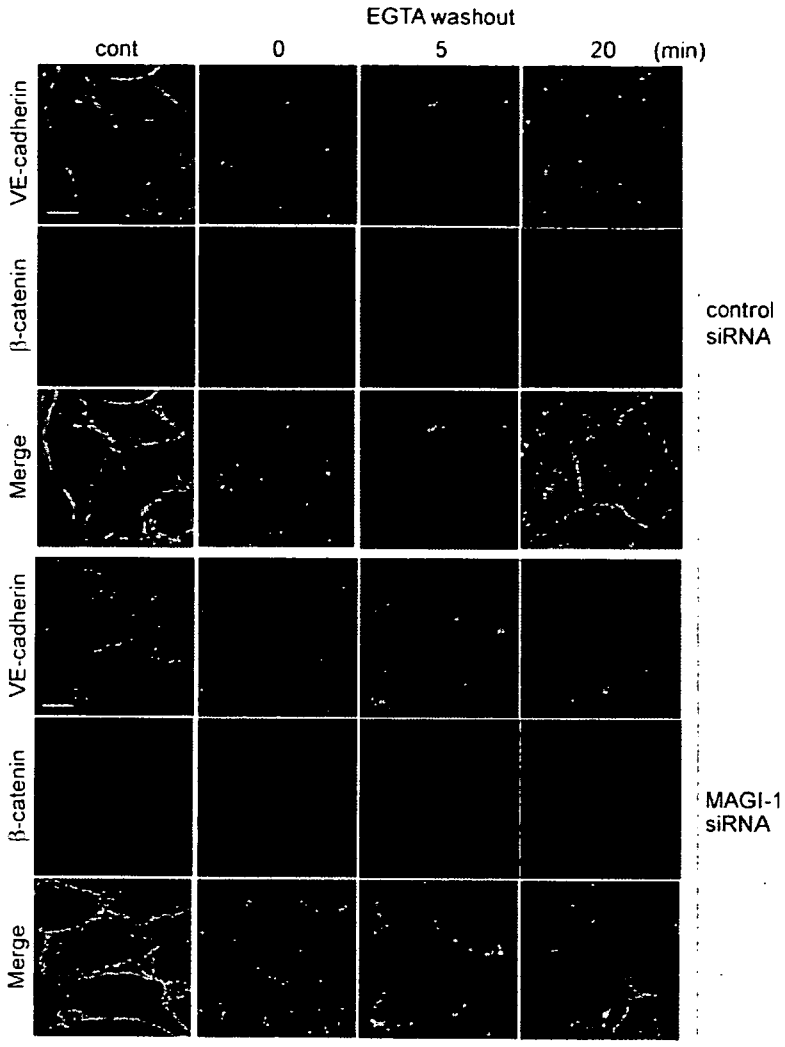

Figure 6. Depletion of MAGI-1 impairs AJ formation. HUVECs transfected with control siRNAs (top three columns) or MAGI-1 siRNAs (bottom three columns) were cultured for 48 h. Cells were replated onto the glass-base dishes for another 24 h to constitute the cell–cell contacts. The cells were treated with EGTA for 30 min to disrupt VE-cadherin-dependent junctions and kept in the replaced medium containing Ca^{2+} for the time indicated at the top. The cells were immunostained with anti-VE-cadherin antibody (green) and anti-β-catenin antibody (red). The merged images are shown in the bottom panels (Merge). Bars, 20 μm. VE-cadherin remarkably accumulated 20 min after Ca^{2+} restoration in control siRNA-treated HUVECs, whereas slight accumulation was observed in MAGI-1 siRNA-treated HUVECs.

These two AJ molecules, VE-cadherin and nectin, are linked by their cytoplasmic domain-associating proteins (Tachibana *et al.*, 2000). L-afadin, a nectin cytoplasmic domain-binding molecule, binds to α-catenin and subsequently locates cadherin to AJs without the transinteraction of cadherin (Tanaka *et al.*, 2003). L-afadin, s-afadin (AF-6), and Canoe (*Drosophila* orthologue of AF-6) contain a Rap1-binding domain (Boettner *et al.*, 2000, 2003). Thus, afadin regulated by activated Rap1 at cell–cell contacts may enhance AJ formation constituted by both cadherin and nectin.

We explored the requirement of MAGI-1 for Rap1 activation at cell adhesion. The association of MAGI-1 with β-catenin via the PDZ domain 5 is critical for its localization to VE-cadherin-based cell–cell contact. MAGI-1 also interacts with endothelial cell-selective adhesion molecule (ESAM) and JAM-4 at TJs (Hirabayashi *et al.*, 2003). Other JAM family members (JAM-A, B, and C) do not bind to MAGI-1 (our unpublished data). The carboxy-terminal sequence of ESAM and JAM-4 provides the class I PDZ-binding motif, whereas that of JAM family members contains the class II PDZ-binding motif (Hung and Sheng, 2002). Thus, ESAM-mediated MAGI-1 recruitment may contribute to Rap1-regulated cell adhesion at TJs as β-catenin recruits MAGI-1 at AJs. It will be interesting to explore the TJ-dependent Rap1 activation.

MAGI-1 together with MAGI-2 (S-SCAM), and MAGI-3 constitute the MAGI family (Hirao *et al.*, 2000; Franklin *et al.*, 2005). It has been shown that MAGI-2 binds to β-catenin and that MAGI-3 colocalized to β-catenin in astrocytes expressing E-cadherin (Adamsky *et al.*, 2003; Subauste *et al.*, 2005). Although MAGI-2 is exclusively expressed in the brain, MAGI-3 is ubiquitously expressed. Although we cannot exclude the involvement of MAGI-3 in the activation of Rap1 in vascular endothelial cells, the disconnection of MAGI family members from β-catenin by overexpressing the PDZ domain 5 of MAGI-1 perturbed the Rap1 activation upon cell–cell contact (Figure 4, D and E). Furthermore, depletion of MAGI-1 by siRNA hampered the Rap1 activation (Figure 5), suggesting that MAGI-1 is indispensable for Rap1 activation based on the linkage between VE-cadherin-β-catenin complex and MAGI-PDZ-GEF1 complex in vascular endothelial cells.

To delineate the VE-cadherin engagement-triggered Rap1 activation signal, we tried to test the requirement of

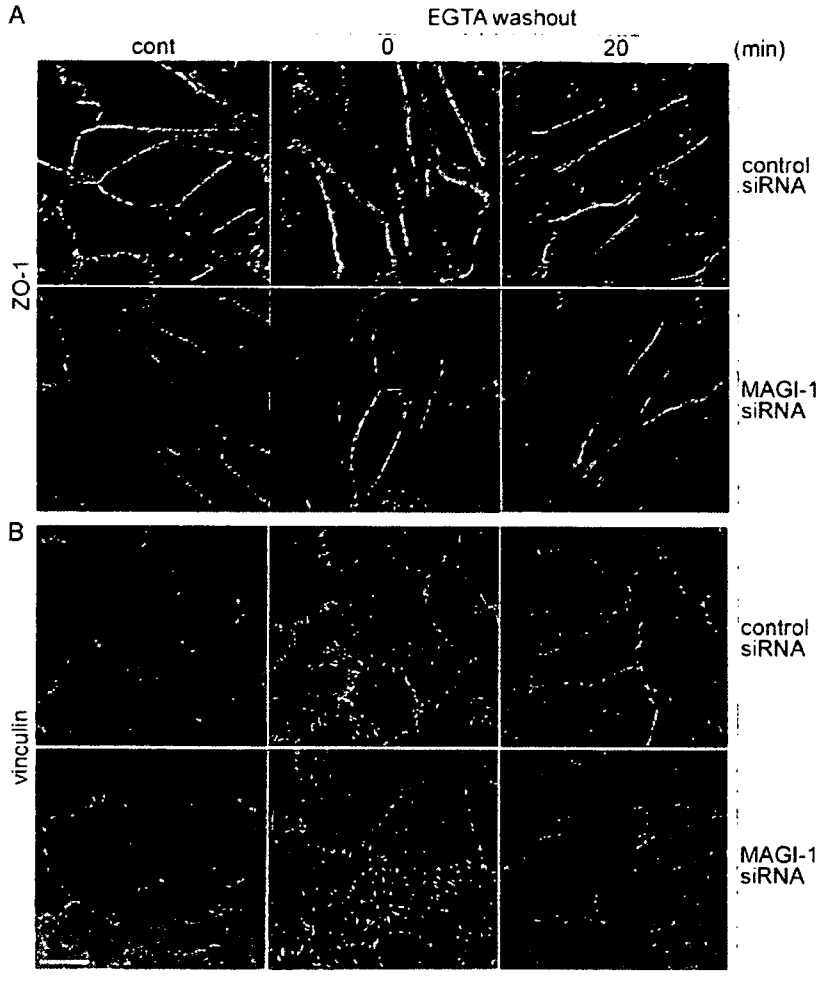

Figure 7. MAGI-1 depletion affects an AJ-supporting molecule, vinculin, but not a TJ-supporting molecule, ZO-1. (A) Similarly to Figure 6, HUVECs treated with control siRNAs (top panels) and MAGI-1 siRNAs (bottom panels) were immunostained with anti-ZO-1 after calcium switch. Bar, 20 μm. Note that ZO-1-positive cells were affected neither by calcium switch nor MAGI-1 depletion. (B) Similarly to A, control siRNA-treated cells and MAGI-1-depleted cells were immunostained with anti-vinculin before and after Ca^{2+} switch. Ca^{2+} depletion from the culture medium resulted in displacement of vinculin from cell–cell contacts to cell-ECM contacts and Ca^{2+}-restoration induced relocalization from cell-ECM contacts to cell–cell contacts in control HUVECs. In clear contrast, vinculin remained at the cell-ECM contacts even 20 min after Ca^{2+} restoration in MAGI-1-depleted cells.

PDZ-GEF1 for Rap1 activation because we found that MAGI-1 associated with PDZ-GEF1 in vascular endothelial cells (Figure 3), as this association reported previously (Dobrosotskaya and James, 2000; Kawajiri *et al.*, 2000). PDZ-GEF1-depleted cells seemed to be detached from the collagen-coated dishes and the adhesive activity to collagen-coated dish was significantly inhibited. Thus we assumed that there might be other signaling besides MAGI-1–PDZ-GEF1-mediated signal for cell adhesion and thus concluded that PDZ-GEF1-depleted cells were not appropriate for further evaluation to delineate the signaling. At least, VE-cadherin engagement-triggered Rap1 activation requires MAGI-1.

Activated Rap1 upon cell–cell contact further strengthens the VE-cadherin-dependent cell–cell adhesion. Rap1 activation is required for VE-cadherin-mediated cell adhesion (Figure 8B). We previously reported that the inside-out signal regulated by cAMP-Epac-Rap1 signal enhances the VE-cadherin-mediated cell–cell contacts by regulating cortical actin (Fukuhara *et al.*, 2005). Although we did not observe significant cortical actin distribution after calcium switch experiment (unpublished data), we noticed that the relocation of vinculin from cell-ECM to cell–cell contacts was inhibited in MAGI-1-depleted cells. Because vinculin supports the cadherin-based cell contacts by linking actin to cytoplasmic domain of cadherin through α-catenin, inhibition of Rap1 activation by MAGI-1 depletion might affect AJ formation. These results imply a positive feedback loop in cell–cell contact regulated by Rap1; namely, cell–cell contact promotes transdimerization of cell surface adhesion molecules, inducing Rap1 activation followed by further tightening of VE-cadherin-mediated cell adhesion.

In conclusion, we revealed that MAGI-1 is required for Rap1 activation upon cell–cell contacts and in turn for AJ formation. The translocation of MAGI-1 to cell–cell contacts is ascribed to its association with β-catenin. The MAGI-1-associating molecule, PDZ-GEF1, may account for Rap1 activation.

ACKNOWLEDGMENTS

We are grateful to M. Matsuda for his advice, plasmids, and virus; K. Kaibuchi for anti-PDZ-GEF1 antibody; J. T. Pearson for his critical reading of this manuscript; and M. Sone, Y. Mizushima, and Y. Matsuura for their technical assistance. This work was supported by grants from the Ministry of Health, Labor, and Welfare Foundation of Japan; from the Program for Promotion of Fundamental Studies in Health Sciences of the National Institute of Biomedical Innovation; from the Ministry of Education, Science, Sports and Culture of Japan; from the Mochida Memorial Foundation for Medical and Pharmaceutical Research; and from Astellas Foundation for Research on Metabolic Disorders.

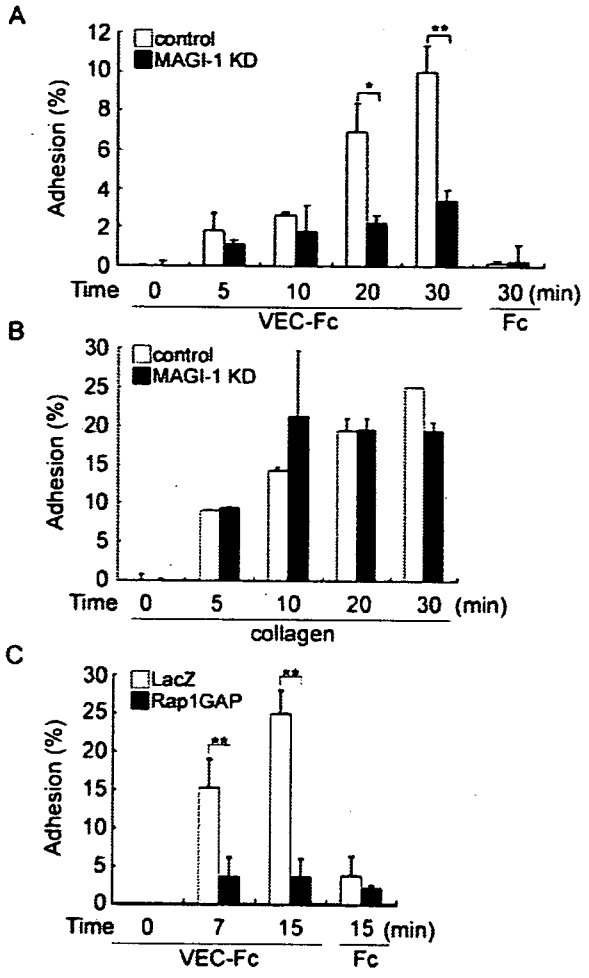

Figure 8. Depletion of MAGI-1 and inactivation of Rap1 inhibits VE-cadherin-mediated cell adhesion. (A) HUVECs transfected with control siRNAs (white column) or MAGI-1 siRNAs (black column) were cultured for 48 h, suspended in 0.5% BSA-containing medium 199, and incubated for 30 min at 37°C. Cells, 2.0×10^5, were plated onto either a VEC-Fc- or Fc-coated well for the time indicated at the bottom. Cell adhesion was quantified as described in *Materials and Methods*. The averages of triplicate (plus SDs) are presented. A representative result of three independent experiments is shown. Statistical significance was analyzed by Student's *t* test ; * $p < 0.05$ and ** $p < 0.01$. Note that adhesion of HUVECs treated with MAGI-1 siRNAs to the VEC-Fc-coated dish was significantly reduced compared with mock-treated HUVECs. (B) Adhesion of MAGI-1-depleted cells to a collagen-coated dish was comparable to mock-treated HUVECs, as analyzed by the same method described in the legend for A. (C) HUVECs infected with either LacZ-expressing adenovirus (LacZ) or Rap1GAPII-expressing virus (Rap1GAP) were analyzed for adhesion to a VEC-Fc-coated dish similarly to A.

REFERENCES

Adamsky, K., Arnold, K., Sabanay, H., and Peles, E. (2003). Junctional protein MAGI-3 interacts with receptor tyrosine phosphatase beta (RPTP beta) and tyrosine-phosphorylated proteins. J. Cell Sci. *116*, 1279–1289.

Boettner, B., Govek, E. E., Cross, J., and Van Aelst, L. (2000). The junctional multidomain protein AF-6 is a binding partner of the Rap1A GTPase and associates with the actin cytoskeletal regulator profilin. Proc. Natl. Acad. Sci. USA *97*, 9064–9069.

Boettner, B., Harjes, P., Ishimaru, S., Heke, M., Fan, H. Q., Qin, Y., Van Aelst, L., and Gaul, U. (2003). The AF-6 homolog canoe acts as a Rap1 effector during dorsal closure of the *Drosophila* embryo. Genetics *165*, 159–169.

Bos, J. L. (2005). Linking Rap to cell adhesion. Curr. Opin. Cell Biol. *17*, 123–128.

Bos, J. L., de Rooij, J., and Reedquist, K. A. (2001). Rap1 signalling: adhering to new models. Nat. Rev. Mol. Cell Biol. *2*, 369–377.

Dejana, E. (2004). Endothelial cell-cell junctions: happy together. Nat. Rev. Mol. Cell Biol. *5*, 261–270.

Dobrosotskaya, I., Guy, R. K., and James, G. L. (1997). MAGI-1, a membrane-associated guanylate kinase with a unique arrangement of protein-protein interaction domains. J. Biol. Chem. *272*, 31589–31597.

Dobrosotskaya, I. Y. (2001). Identification of mNET1 as a candidate ligand for the first PDZ domain of MAGI-1. Biochem. Biophys. Res. Commun. *283*, 969–975.

Dobrosotskaya, I. Y., and James, G. L. (2000). MAGI-1 interacts with beta-catenin and is associated with cell-cell adhesion structures. Biochem. Biophys. Res. Commun. *270*, 903–909.

Esser, S., Lampugnani, M. G., Corada, M., Dejana, E., and Risau, W. (1998). Vascular endothelial growth factor induces VE-cadherin tyrosine phosphorylation in endothelial cells. J. Cell Sci. *111*(Pt 13), 1853–1865.

Franke, B., Akkerman, J. W., and Bos, J. L. (1997). Rapid Ca2+-mediated activation of Rap1 in human platelets. EMBO J. *16*, 252–259.

Franklin, J. L., Yoshiura, K., Dempsey, P. J., Bogatcheva, G., Jeyakumar, L., Meise, K. S., Pearsall, R. S., Threadgill, D., and Coffey, R. J. (2005). Identification of MAGI-3 as a transforming growth factor-alpha tail binding protein. Exp. Cell Res. *303*, 457–470.

Fukuhara, S., Sakurai, A., Sano, H., Yamagishi, A., Somekawa, S., Takakura, N., Saito, Y., Kangawa, K., Mochizuki, N. (2005). Cyclic AMP potentiates vascular endothelial cadherin-mediated cell-cell contact to enhance endothelial barrier function through an Epac-Rap1 signaling pathway. Mol. Cell Biol. *25*, 136–146.

Fukuyama, T., Ogita, H., Kawakatsu, T., Fukuhara, T., Yamada, T., Sato, T., Shimizu, K., Nakamura, T., Matsuda, M., and Takai, Y. (2005). Involvement of the c-Src-Crk-C3G-Rap1 signaling in the nectin-induced activation of Cdc42 and formation of adherens junctions. J. Biol. Chem. *280*, 815–825.

Herren, B., Levkau, B., Raines, E. W., and Ross, R. (1998). Cleavage of beta-catenin and plakoglobin and shedding of VE-cadherin during endothelial apoptosis: evidence for a role for caspases and metalloproteinases. Mol. Biol. Cell *9*, 1589–1601.

Hirabayashi, S., Tajima, M., Yao, I., Nishimura, W., Mori, H., and Hata, Y. (2003). JAM4, a junctional cell adhesion molecule interacting with a tight junction protein, MAGI-1. Mol. Cell Biol. *23*, 4267–4282.

Hirao, K., Hata, Y., Ide, N., Takeuchi, M., Irie, M., Yao, I., Deguchi, M., Toyoda, A., Sudhof, T. C., and Takai, Y. (1998). A novel multiple PDZ domain-containing molecule interacting with N-methyl-D-aspartate receptors and neuronal cell adhesion proteins. J. Biol. Chem. *273*, 21105–21110.

Hirao, K., Hata, Y., Yao, I., Deguchi, M., Kawabe, H., Mizoguchi, A., and Takai, Y. (2000). Three isoforms of synaptic scaffolding molecule and their characterization. Multimerization between the isoforms and their interaction with N-methyl-D-aspartate receptors and SAP90/PSD-95-associated protein. J. Biol. Chem. *275*, 2966–2972.

Hogan, C., Serpente, N., Cogram, P., Hosking, C. R., Bialucha, C. U., Feller, S. M., Braga, V. M., Birchmeier, W., and Fujita, Y. (2004). Rap1 regulates the formation of E-cadherin-based cell-cell contacts. Mol. Cell Biol. *24*, 6690–6700.

Hudry-Clergeon, H., Stengel, D., Ninio, E., and Vilgrain, I. (2005). Platelet-activating factor increases VE-cadherin tyrosine phosphorylation in mouse endothelial cells and its association with the PtdIns3′-kinase. FASEB J. *19*, 512–520.

Hung, A. Y., and Sheng, M. (2002). PDZ domains: structural modules for protein complex assembly. J. Biol. Chem. *277*, 5699–5702.

Ide, N., Hata, Y., Deguchi, M., Hirao, K., Yao, I., and Takai, Y. (1999). Interaction of S-SCAM with neural plakophilin-related Armadillo-repeat protein/delta-catenin. Biochem. Biophys. Res. Commun. *256*, 456–461.

Iyer, S., Ferreri, D. M., DeCocco, N. C., Minnear, F. L., and Vincent, P. A. (2004). VE-cadherin-p120 interaction is required for maintenance of endothelial barrier function. Am. J. Physiol Lung Cell Mol. Physiol. *286*, L1143–L1153.

Kawajiri, A., Itoh, N., Fukata, M., Nakagawa, M., Yamaga, M., Iwamatsu, A., and Kaibuchi, K. (2000). Identification of a novel beta-catenin-interacting protein. Biochem. Biophys. Res. Commun. *273*, 712–717.

Knox, A. L., and Brown, N. H. (2002). Rap1 GTPase regulation of adherens junction positioning and cell adhesion. Science *295*, 1285–1288.

Kobielak, A., and Fuchs, E. (2004). Alpha-catenin: at the junction of intercellular adhesion and actin dynamics. Nat. Rev. Mol. Cell Biol. *5*, 614–625.

Kogata, N., Masuda, M., Kamioka, Y., Yamagishi, A., Endo, A., Okada, M., and Mochizuki, N. (2003). Identification of Fer tyrosine kinase localized on microtubules as a platelet endothelial cell adhesion molecule-1 phosphorylating kinase in vascular endothelial cells. Mol. Biol. Cell *14*, 3553–3564.

Kooistra, M. R., Corada, M., Dejana, E., and Bos, J. L. (2005). Epac1 regulates integrity of endothelial cell junctions through VE-cadherin. FEBS Lett. *579*, 4966–4972.

Kotelevets, L., van Hengel, J., Bruyneel, E., Mareel, M., van Roy, F., and Chastre, E. (2005). Implication of the MAGI-1b/PTEN signalosome in stabilization of adherens junctions and suppression of invasiveness. FASEB J. *19*, 115–117.

Laura, R. P., Ross, S., Koeppen, H., and Lasky, L. A. (2002). MAGI-1, a widely expressed, alternatively spliced tight junction protein. Exp. Cell Res. *275*, 155–170.

Mandell, K. J., Babbin, B. A., Nusrat, A., and Parkos, C. A. (2005). Junctional adhesion molecule 1 regulates epithelial cell morphology through effects on beta1 integrins and Rap1 activity. J. Biol. Chem. *280*, 11665–11674.

Mino, A., Ohtsuka, T., Inoue, E., and Takai, Y. (2000). Membrane-associated guanylate kinase with inverted orientation (MAGI)-1/brain angiogenesis inhibitor 1-associated protein (BAP1) as a scaffolding molecule for Rap small G protein GDP/GTP exchange protein at tight junctions. Genes Cells *5*, 1009–1016.

Mochizuki, N., Yamashita, S., Kurokawa, K., Ohba, Y., Nagai, T., Miyawaki, A., and Matsuda, M. (2001). Spatio-temporal images of growth-factor-induced activation of Ras and Rap1. Nature *411*, 1065–1068.

Nagashima, K., Endo, A., Ogita, H., Kawana, A., Yamagishi, A., Kitabatake, A., Matsuda, M., Mochizuki, N. (2002). Adaptor protein Crk is required for Ephrin-B1-induced membrane ruffling and focal complex assembly of human aortic endothelial cells. Mol. Biol. Cell *13*, 4231–4242.

Navarro, P., Ruco, L., and Dejana, E. (1998). Differential localization of VE- and N-cadherins in human endothelial cells: VE-cadherin competes with N-cadherin for junctional localization. J. Cell Biol. *140*, 1475–1484.

Nwariaku, F. E., Liu, Z., Zhu, X., Nahari, D., Ingle, C., Wu, R. F., Gu, Y., Sarosi, G., and Terada, L. S. (2004). NADPH oxidase mediates vascular endothelial cadherin phosphorylation and endothelial dysfunction. Blood *104*, 3214–3220.

Ohba, Y. *et al.* (2001). Requirement for C3G-dependent Rap1 activation for cell adhesion and embryogenesis. EMBO J. *20*, 3333–3341.

Price, L. S., Hajdo-Milasinovic, A., Zhao, J., Zwartkruis, F. J., Collard, J. G., and Bos, J. L. (2004). Rap1 regulates E-cadherin-mediated cell-cell adhesion. J. Biol. Chem. *279*, 35127–35132.

Subauste, M. C., Nalbant, P., Adamson, E. D., and Hahn, K. M. (2005). Vinculin controls PTEN protein level by maintaining the interaction of the adherens junction protein beta-catenin with the scaffolding protein MAGI-2. J. Biol. Chem. *280*, 5676–5681.

Tachibana, K., Nakanishi, H., Mandai, K., Ozaki, K., Ikeda, W., Yamamoto, Y., Nagafuchi, A., Tsukita, S., and Takai, Y. (2000). Two cell adhesion molecules, nectin and cadherin, interact through their cytoplasmic domain-associated proteins. J. Cell Biol. *150*, 1161–1176.

Tanaka, Y., Nakanishi, H., Kakunaga, S., Okabe, N., Kawakatsu, T., Shimizu, K., and Takai, Y. (2003). Role of nectin in formation of E-cadherin-based adherens junctions in keratinocytes: analysis with the N-cadherin dominant negative mutant. Mol. Biol. Cell *14*, 1597–1609.

Volberg, T., Geiger, B., Kartenbeck, J., and Franke, W. W. (1986). Changes in membrane-microfilament interaction in intercellular adherens junctions upon removal of extracellular Ca2+ ions. J. Cell Biol. *102*, 1832–1842.

Wittchen, E. S., Worthylake, R. A., Kelly, P., Casey, P. J., Quilliam, L. A., and Burridge, K. (2005). Rap1 GTPase inhibits leukocyte transmigration by promoting endothelial barrier function. J. Biol. Chem. *280*, 11675–11682.

Yamada, A., Irie, K., Hirota, T., Ooshio, T., Fukuhara, A., and Takai, Y. (2005). Involvement of the annexin II-S100A10 complex in the formation of E-cadherin-based adherens junctions in Madin-Darby canine kidney cells. J. Biol. Chem. *280*, 6016–6027.

Zanetti, A., Lampugnani, M. G., Balconi, G., Breviario, F., Corada, M., Lanfrancone, L., and Dejana, E. (2002). Vascular endothelial growth factor induces SHC association with vascular endothelial cadherin: a potential feedback mechanism to control vascular endothelial growth factor receptor-2 signaling. Arterioscler. Thromb. Vasc. Biol. *22*, 617–622.

THE JOURNAL OF BIOLOGICAL CHEMISTRY VOL. 281, NO. 52, pp. 40242–40251, December 29, 2006

Interaction of FoxO1 and TSC2 Induces Insulin Resistance through Activation of the Mammalian Target of Rapamycin/p70 S6K Pathway*

Received for publication, August 23, 2006, and in revised form, October 30, 2006 Published, JBC Papers in Press, October 31, 2006, DOI 10.1074/jbc.M608116200

Yongheng Cao[‡], Yuji Kamioka[§], Norihide Yokoi[¶], Toshiyuki Kobayashi[‖], Okio Hino[‖], Masafumi Onodera[**], Naoki Mochizuki[§], and Jun Nakae[‡1]

From the [‡]Department of Clinical Molecular Medicine, Division of Diabetes, Digestive and Kidney Disease, Kobe University Graduate School of Medicine, Kobe 650-0017, the [§]Department of Structural Analysis, National Cardiovascular Center Research Institute, 5-7-1 Fujishirodai, Suita, Osaka 565-8565, [¶]Division of Cellular and Molecular Medicine, Kobe University Graduate School of Medicine, Kobe 650-0017, the [‖]Department of Experimental Pathology, Cancer Institute, Japanese Foundation for Cancer Research, 1-37-1 Kami-ikebukuro, Toshima-ku, Tokyo 170-8455, and [**]Advanced Biomedical Applications, Graduate School of Comprehensive Human Sciences, University of Tsukuba, Tsukuba 305-8575, Japan

Both TSC2 (tuberin) and forkhead transcription factor FoxO1 are phosphorylated and inhibited by Akt and play important roles in insulin signaling. However, little is known about the relationship between TSC2 and FoxO1. Here we identified TSC2 as a FoxO1-binding protein by using a yeast two-hybrid screening with a murine islet cDNA library. Among FoxOs, only FoxO1 can be associated with TSC2. The physical association between the C terminus of TSC2 (amino acids 1280–1499) and FoxO1 degrades the TSC1-TSC2 complex and inhibits GTPase-activating protein activity of TSC2 toward Rheb. Overexpression of wild type FoxO1 enhances p70 S6K phosphorylation, whereas overexpression of TSC2 can reverse these effects. Knockdown of endogenous FOXO1 in human vascular endothelial cells decreased phosphorylation of p70 S6K. Prolonged overexpression of wild type FoxO1 enhanced phosphorylation of serine 307 of IRS1 and decreased phosphorylation of Akt and FoxO1 itself even in the presence of serum. These data suggest a novel mechanism by which FoxO1 regulates the insulin signaling pathway through negative regulation of TSC2 function.

Forkhead transcription factors of the FoxO (Forkhead box-containing protein, O subfamily) family are conserved across many species. In *Caenorhabditis elegans*, DAF-16, the FoxO orthologue, is downstream of the DAF-2/AGE-1/AKT signaling pathway (1, 2). Loss-of-function of *daf-2*, *age-1*, or *akt* causes life span extension in a *daf-16*-dependent manner (3). In *Drosophila*, the life span is extended over 50% by ablation of insulin-producing cells or mutations of genes encoding the insulin-like receptor (*dInR*) or its receptor substrate (*chico*) (4). Similarly, dInR phosphorylates and inactivates dFOXO, the *Drosophila* homologue of DAF-16/FOXO (5). In mammals, InsR/IGF1R-PI3K-Akt signaling inhibits transcription by FoxO1, FoxO3a, and FoxO4 (6). These proteins possess a forkhead DNA binding domain consisting of around 110 amino acids and a transactivation domain in the C terminus. FoxOs bind to consensus FoxO-binding sites (GTAAA(C/T)A, T(G/A)TTTAC) in the promoter region of their target genes and activate gene expression (7). It has been reported that FoxOs cause cell cycle arrest through induction of *p27*, *p21*, cyclin B, *polo-like kinase*, the retinoblastoma family-related protein p130 and cyclin G2, apoptosis through induction of *Fas* ligand and *Bim*, DNA repair through *GADD45*, stress resistance through MnSOD, and regulation of glucose and lipid metabolism through *G6pase*, *apoC-III*, and *Igfbp-1* (8). Several FoxO-binding proteins, which include co-activators, transcription factors, signaling molecules, and Sirt1, a NAD-dependent deacetylase, have also been identified (8). These FoxO-binding molecules regulate FoxO-dependent transcription and vice versa. However, there have been few reports that described identification of FoxO-binding proteins by comprehensive strategies.

The PI3K[2]-Akt pathway is also important for growth factor stimulation of mammalian target of rapamycin (mTOR) signaling (9). The primary mechanism by which Akt activates mTOR signaling appears to be through direct phosphorylation and inhibition of TSC2 (also known as tuberin). TSC1 (also known as hamartin) and TSC2 were first identified as genes mutated in patients with tuberous sclerosis complex (TSC), an autosomal dominant disease. Affected patients suffer from hamartomas in a wide spectrum of organs. TSC1 and TSC2 physically associate *in vivo* and form a heterodimeric complex (10–12). TSC2 has been directly linked to cell size regulation by the discovery that mutation in dTsc2 leads to the gigas (large cell) phenotype (13).

* This work was supported by the 21st Century COE Program "Center of Excellence for Signal Transduction Disease: Diabetes Mellitus as a Model" grant from the Ministry of Education, Culture, Sports, Science and Technology of Japan. The costs of publication of this article were defrayed in part by the payment of page charges. This article must therefore be hereby marked "*advertisement*" in accordance with 18 U.S.C. Section 1734 solely to indicate this fact.

[1] To whom correspondence should be addressed: Dept. of Clinical Molecular Medicine, Division of Diabetes, Digestive and Kidney Diseases, Kobe University Graduate School of Medicine, 7-5-1 Kusunoki-cho, Chuo-ku, Kobe 650-0017, Japan. Tel.: 81-78-382-5374; Fax: 81-78-382-5379; E-mail: nakaej@med.kobe-u.ac.jp.

[2] The abbreviations used are: PI3K, phosphatidylinositol 3-kinase; mTOR, mammalian target of rapamycin; TSC, tuberous sclerosis complex; DMEM, Dulbecco's modified Eagle's medium; HUVEC, human vascular endothelial cell; siRNA, small interfering RNA; RNAi, RNA interference; ANOVA, analysis of variance; WT, wild type; EGFP, enhanced green fluorescent protein; GST, glutathione S-transferase; GAP, GTPase-activating protein; HA, hemagglutinin.

Recent studies revealed that the TSC1-TSC2 complex functions downstream of Akt and upstream of target of rapamycin to restrict cell growth and cell proliferation (14–17). Akt-phosphorylation of TSC2 leads to the functional inactivation of the TSC1-TSC2 complex and results in mTOR activation leading to phosphorylation of two main mTOR substrates, ribosomal p70 S6 kinase (p70 S6K) and eukaryotic initiation factor 4E-binding protein (4E-BP1), and elevated mRNA translation (18–20). The TSC2 C-terminal region has homology with the catalytic domain of GTPase-activating proteins (GAPs). An inhibitory target of TSC1-TSC2 has been identified as Ras homologue enriched in brain (Rheb), a small GTPase. GTP-bound Rheb is bound to and activates mTOR (21, 22).

There have been several reports about molecules, which regulate TSC2 function. Energy depletion inhibits mTOR signaling through AMP-activated kinase phosphorylation of TSC2, although it is not know how AMP-activated kinase phosphorylation of TSC2 enhances the ability of TSC1–TSC2 to inhibit downstream signaling to Rheb (23–25). The hypoxia-inducible gene, regulated in development and damage responses (REDD1), is also induced by energy depletion, and this leads to inhibition of mTOR complex 1 signaling to p70 S6K in a TSC2-dependent manner (26). It is important to identify molecules that regulate TSC2 function because these molecules may affect the activity of mTOR/p70 S6K signaling and finally determine the activity of PI3K/Akt pathway through a negative feedback loop (27).

In this study, we identified TSC2 as a novel FoxO1-binding protein by a yeast two-hybrid screening using a murine islet cDNA library. Binding of FoxO1 to TSC2 in cytoplasm inhibits TSC2 function and results in activation mTOR/p70 S6K and inhibition of Akt activity through negative feedback on IRS protein, leading eventually to feedback activation of FoxO1. Here we demonstrate a novel mechanism by which FoxO1 regulates activity of mTOR/p70 S6K signaling pathway and of FoxO1 itself through association with TSC2.

EXPERIMENTAL PROCEDURES

Antibodies and Plasmids—We purchased anti-FLAG (M2) and anti-tubulin from Sigma; anti-c-Myc (9E10), anti-TSC2 (C-20 and N-19), anti-FOXO1 (H128), anti-FOXO1 (N18), anti-IRS2 from Santa Cruz Biotechnology; anti-HA (12CA5) from Roche Applied Science; anti-p70 S6K, anti-phospho-p70 S6K (Thr(P)-389), anti-phospho-FOXO1 (Ser(P)-256), anti-Akt, anti-phospho-Akt (Thr(P)-308 and Ser(P)-473), and anti-phospho-IRS-1 (Ser(P)-307) from Cell Signaling Technology; anti-TSC1 from Zymed Laboratories Inc.; anti-IRS1 from Upstate Biotechnology, Inc.; and anti-GFP from Dr. Michiyuki Matsuda, Osaka University. We used pCAG/FLAG-rTSC2DEE, pMT2/FLAG-p70 S6K (28), pCMV5/cMyc/FoxO1 (29), pCMV5/cMyc/FoxO3a (30), pTB701-FLAG-FOXO4 (31), pCA-EGFP-Rheb (32), and adenoviral vectors encoding wild type or mutant FoxO1 (30). The pCAG/FLAG-rTSC2DEE was constructed by ligation of N-terminal FLAG-tagged full-length cDNA of rTSC2 with pCAG-GS vector (33, 34).

Construction of Expression Vectors—For mutagenesis of FoxO1, we performed overlap extension PCR using pCMV5/cMyc/ADA FoxO1 as a template as described previously (35). For construction of pCMV5/cMyc/T24A/S253A/S316A (3A), the following mutagenic primers were used: primer 1, 5′-AGA GCT GCG GCC ATG GAC AAC-3′, corresponding to nucleotide 844–864, and primer 2, 5′-GTT GTC CAT GGC CGC AGC TCT-3′, corresponding to nucleotide 864–844.

Yeast Two-hybrid Screen—Amino acids 424–550 of the murine FoxO1 were cloned in-frame into the GAL4 DNA-binding domain plasmid pGBKT7 (Clontech). The GAL4 activation domain cDNA library of murine islets was constructed as described previously (36). AH109 yeast strain was used for the library search. The transformation was performed as described in the Clontech Matchmaker two-hybrid system 3 protocol. The transformants were plated on SD/−Ade/−His/−Leu/−Tyr plates in the presence of galactose and then were incubated at 30 °C for 3–4 days. Positive interaction was identified by strong β-galactosidase activity. Individual positive clones were isolated by YEASTMAKER™ yeast plasmid isolation kit (BD Biosciences) and were sequenced by ABI310 automated DNA sequencer and analyzed for homology with sequences in the GenBank™ data base using the BLAST algorithm.

Cell Culture, Transfection, and Viral Transduction—HEK293 cells were cultured in DMEM containing 10% fetal calf serum. SV40-transformed hepatocytes used in these studies have been described in previous publication (29). Human vascular endothelial cells (HUVEC) were cultured in HuMedia-EB2 (KURABO) supplemented with 2% fetal calf serum, 10 ng/ml human recombinant epidermal growth factor, 1 μg/ml hydrocortisone, 5 ng/ml human recombinant fibroblast growth factor, and 10 μg/ml heparin. Transient transfection was performed using Lipofectamine (Invitrogen) according to manufacturer's protocol. Adenoviral infection was described in a previous publication (30). We transduced SV40-transformed hepatocytes by incubating them with adenoviral preparations at 10–50 multiplicities of infection for 2 h.

Cell Isolation and Culture—Brown adipocytes and their precursor cells were isolated from newborn wild type mice by collagenase digestion as described previously (37). Preadipocytes were immortalized by infection with the retroviral vector pGCDNsamIRES-Puro, encoding SV40T antigen (38) and selected with puromycin (1 μg/ml). Preadipocytes were grown to confluence in culture medium supplemented with 50 nM insulin and 50 nM triiodothyronine (differentiation medium) (day 0). Adipocyte differentiation was induced by treating confluent cells for 24 h in differentiation medium further supplemented with 0.5 mM isobutylmethylxanthine, 0.5 μM dexamethasone, and 0.125 mM indomethacin. After induction, cells were changed back to differentiation medium, which was then changed every day. At day 5, cells were harvested and used for experiments.

Western Blot Analysis—We lysed cells in buffer containing 50 mM Tris-HCl (pH 7.6), 250 mM NaCl, 1% Nonidet P-40, 0.5% deoxycholate, 0.1% SDS, and protease inhibitors (Roche Applied Science). After centrifugation to remove insoluble material, each 30 μg of sample was electrophoresed in SDS-PAGE, and Western blotting was performed. For immunoprecipitation, cell lysates were diluted with buffer containing 50

mM Tris-HCl (pH 7.6), 150 mM NaCl, 0.1% Nonidet P-40, 10% glycerol, 5 mM $MgCl_2$, and protease inhibitors.

In Vitro Translation and Glutathione S-Transferase Fusion Protein Pulldown Assay—The TSC2 deletions were generated by PCR using specific primers, and they were cloned in-frame into the EcoRI and SalI sites of pGEX-4T-1. These fusion proteins were expressed in 20 μl of 50% slurry beads containing ~2 μg of protein (either GST or alone, or fused to deleted TSC2 mutants), resuspended in 350 μl of binding buffer (50 mM Tris-HCl (pH 8.0), 120 mM NaCl, 1 mM EDTA, and 0.5% Nonidet P-40). This was mixed with 10 μl of *in vitro* translated wild type FoxO1 (Promega TNT reticulocyte lysate system kit). Binding was performed for 6 h at 4 °C. The beads were then washed four times with the binding buffer and resuspended in 2× SDS-PAGE sample buffer. Samples were then subjected to SDS-PAGE and transferred to a nitrocellulose membrane; the blot was incubated with anti-FOXO1 antibody and developed with an ECL detection system (Amersham Biosciences).

Immunofluorescence—Immunofluorescence using SV40-transformed hepatocytes was performed as described previously (35). After transient transfection with pCAG/FLAG-TSC2 using Lipofectamine (Invitrogen), SV40-transformed hepatocytes were transduced with adenovirus encoding HA-tagged wild type or ADA-FoxO1. HA-tagged FoxO1 was visualized with anti-HA monoclonal antibody and fluorescein isothiocyanate-conjugated anti-mouse IgG, and TSC2 was visualized with anti-TSC2 polyclonal antibody and rhodamine-conjugated anti-rabbit IgG.

Measurement of GTP- and GDP-bound Rheb—SV40-transformed hepatocytes were cultured in 6-well plates and co-transfected with pCAG/FLAG-rTSC2DEE and pCA-EGFP-Rheb using Lipofectamine 2000 reagent (Invitrogen) and subsequently transduced with an adenovirus encoding WT FoxO1. At 48 h after transfection, the cells were washed once with phosphate-free DMEM (DMEM without sodium phosphate and sodium pyruvate; Invitrogen) and incubated with 1 ml of phosphate-free DMEM for 90 min. Cells were then incubated with 25 μCi of [^{32}P]phosphate/ml (GE healthcare) for 4 h. After the labeling, cells were lysed with prechilled lysis buffer (0.5% Triton X-100, 20 mM Tris (pH 7.5), 150 mM NaCl, 20 mM $MgCl_2$, 1 mM phenylmethylsulfonyl fluoride, 10 μg of leupeptin/ml, 10 μg of aprotinin/ml; 600 μl per well of a 6-well plate). To avoid lysing the nuclei, the cells were incubated with lysis buffer for just 30 s with gentle shaking. The lysates were then centrifuged at 12,000 × *g* for 15 min at 4 °C. The supernatant (500 μl) was transferred to a fresh tube. Sixteen microliters of NaCl (500 mM) was added to 160 μl of supernatant to inhibit GAP activity in the lysates. To immunoprecipitate pCA-EGFP-Rheb, anti-green fluorescent protein and protein A-agarose (GE Healthcare) were added to the supernatant and incubated for 3 h at 4 °C. The beads were washed with lysis buffer two times and with wash buffer (20 mM Tris (pH 7.5), 150 mM NaCl, 20 mM $MgCl_2$) one time at 4 °C. The Rheb-bound nucleotides were eluted with 15 μl of elution buffer (20 mM Tris (pH 7.5), 20 mM EDTA, 2% SDS) at 68 °C for 10 min. Ten microliters of eluted nucleotides was then applied onto polyethyleneimine-cellulose plates. Before applying sample, the plate was soaked in methanol and dried with a hair dryer. The bottom portion of the plate was immersed in methanol again, and the plate was placed in a sealed chromatography chamber that was filled with 0.75 M KH_2PO_4 (pH 3.4) to a depth of 1 cm. The chamber was closed, and the solvent was allowed to ascend to the top of the plate. The plate was then removed and air-dried. GTP and GDP resolved by thin layer chromatography were visualized and quantified by a BAS-5000 (Fuji Film).

Design and Transfection of siRNAs—We used BLOCK iT RNAi Designer (Invitrogen) to identify target siRNAs and used Stealth RNAi (Invitrogen). The FOXO1-specific sequence was 5′-AACUGCAGAUGUCUGCUGAGCAUGU-3′. HUVECs were transfected with Stealth RNAi using Lipofectamine 2000 according to the manufacturer's instruction (Invitrogen). At 48 h after transfection, cells were harvested and used for Western blotting.

Statistics—We calculated descriptive statistics and ANOVA followed by Fisher's test using the Statview software (SAS Institute Inc.).

RESULTS

Identification of TSC2 as a FoxO1-binding Protein—To identify proteins that bind to FoxO1, we performed a yeast two-hybrid screen using GAL4-FoxO1 fragment (amino acids 424–550) as bait and a murine islet cDNA library as prey. About 2 × 10^6 transformants were tested. The strongest colony was isolated and was found to encode the C-terminal fragment of murine TSC2 (amino acids 1280–1815). To confirm the interaction between TSC2 and FoxO1, we co-transfected HEK293 cells with pCAG/FLAG-rTSC2DEE and pCMV5/cMyc-WT FoxO1, and we immunoprecipitated cell lysates using normal mouse IgG or anti-c-Myc mouse antibody and blotted with anti-FLAG antibody. Reciprocal immunoprecipitation/immunoblotting using anti-FLAG and anti-c-Myc antibodies showed that the exogenously expressed FoxO1 could interact with FLAG-tagged full-length-TSC2 (Fig. 1*a*).

Furthermore, to investigate whether endogenous FoxO1 is physically associated with TSC2 or not, cell lysates from brown adipocytes immortalized by SV40-T antigen were immunoprecipitated with anti-FOXO1 (Fig. 1*b*, *lane 2*) or anti-TSC2 (Fig. 1*b*, *lane 5*) and followed by an immunoblotting with using antibodies against TSC2 (Fig. 1*b*, *lanes 1–3, top panel*) or FOXO1 (Fig. 1*b*, *lanes 4–6, top panel*). In this cell line, both FoxO1 and TSC2 are expressed abundantly. Our results showed that endogenous FoxO1 was associated with endogenous TSC2 (Fig. 1*b*). These results suggest that FoxO1 interacts physically with TSC2 *in vivo*.

TSC2 Binds to Only FoxO1 among FoxO Family Members—FoxOs consist of FoxO1, FoxO3a, and FoxO4. These molecules have highly conserved motifs, which include forkhead DNA binding domain, three Akt phosphorylation sites, and several acetylation sites. Therefore, it is interesting to investigate whether TSC2 is associated with other FoxOs or not. To examine whether all three FoxOs can interact with TSC2 equally, we transfected SV40-transformed hepatocytes with cMyc-FoxO1, -FoxO3a, or FLAG-FOXO4 and immunoprecipitated lysates with antibody against TSC2 or normal rabbit serum and immunoblotted with antibody against c-Myc or FLAG. This co-immunoprecipitation study demonstrated that only FoxO1 could

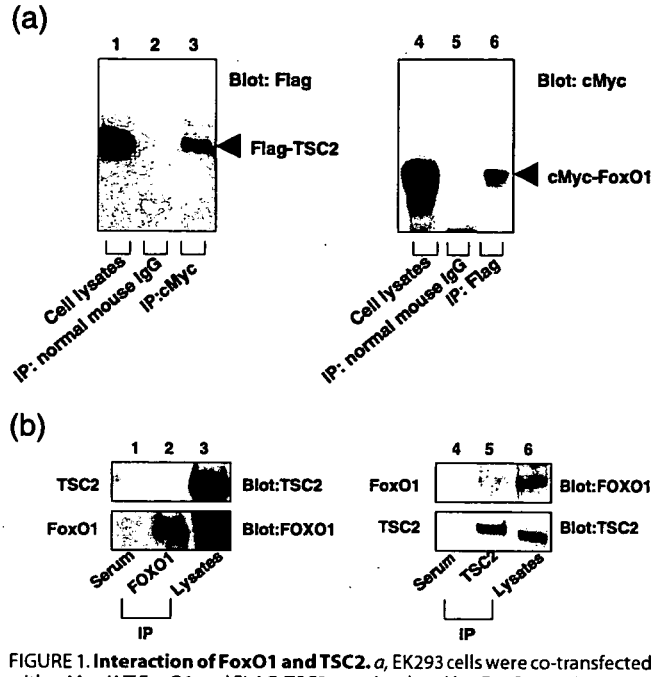

FIGURE 1. **Interaction of FoxO1 and TSC2.** *a*, EK293 cells were co-transfected with c-Myc-WT FoxO1 and FLAG-TSC2 transiently. c-Myc FoxO1 was immunoprecipitated (*IP*) with anti-c-Myc mouse monoclonal antibody (*lane 3*) or normal mouse IgG (*lane 2*), and the immune complexes were assessed for the presence of FLAG-TSC2 by Western blotting (*Blot*) with anti-FLAG antibody. Reciprocal experiment was done by immunoprecipitation with anti-FLAG (*lane 6*) or normal mouse IgG (*lane 5*) and Western blotting with anti-c-Myc antibody. *b*, cell lysates from immortalized brown adipocytes were immunoprecipitated with normal rabbit serum (*lanes 1* and *4*), anti-FOXO1 (*lane 2*), or anti-TSC2 rabbit polyclonal antibody (*lane 5*) and immunoblotted with anti-TSC2 (the *upper panel* from *lanes 1–3*) or anti-FOXO1 goat polyclonal antibody (N18) (the *upper panel* from *lanes 4–6*).

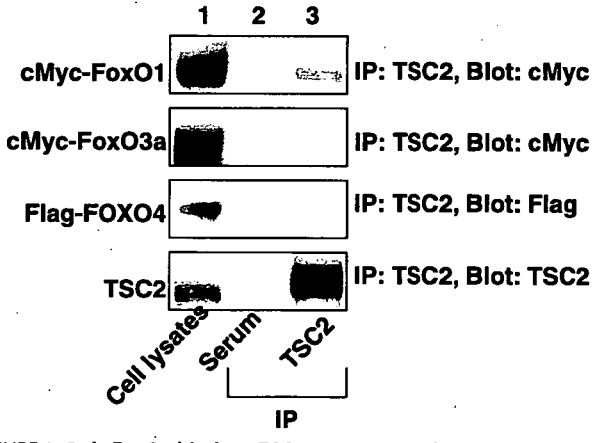

FIGURE 2. **Only FoxO1 binds to TSC2 among FoxO family members.** Cell lysates from SV40-transformed hepatocytes transfected with c-Myc-FoxO1 (*top panel*), -FoxO3a (*2nd panel*), or FLAG-FOXO4 (*3rd panel*) were immunoprecipitated (*IP*) with normal rabbit serum (*lane 2*) or anti-TSC2 rabbit polyclonal antibody (*lane 3*) and immunoblotted with anti-c-Myc mouse (*top* and *2nd panels*) or anti-FLAG mouse monoclonal antibody (*3rd panel*).

interact with endogenous TSC2 (Fig. 2, *lane 3, top panel*). These data suggest that FoxO1 interacts with TSC2 among FoxOs specifically.

Identification of FoxO1-binding Site in TSC2 Protein—To examine whether FoxO1 interacts with TSC2 directly, we constructed several glutathione *S*-transferase (GST) fusion TSC2

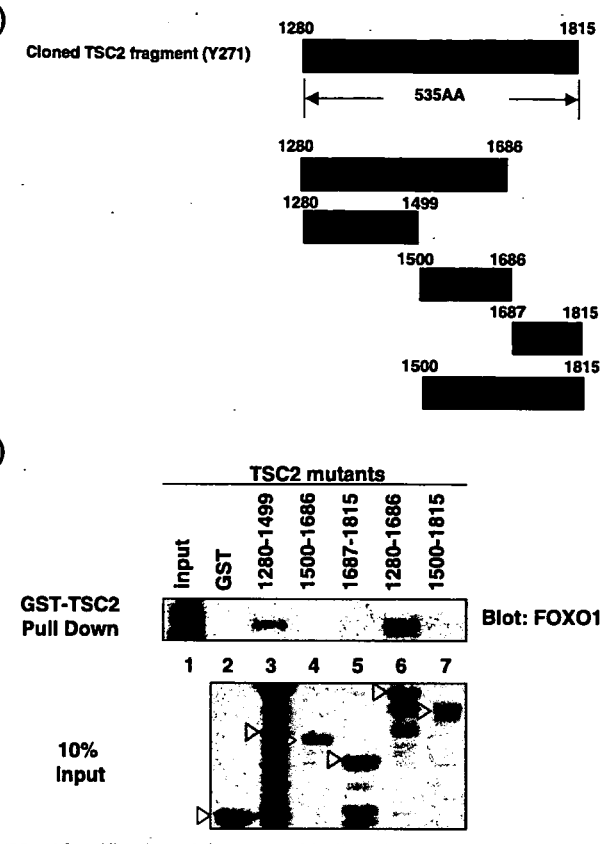

FIGURE 3. **Identification of the FoxO1-binding site in TSC2.** *a*, schematics of TSC2 deletion mutants are shown. The top deleted mutant fragment of TSC2 is cloned by a yeast two-hybrid assay. *b*, GST-TSC2 deleted mutants, indicated by *arrowheads*, were subjected to pulldown assay. Aliquots of *in vitro* translated wild type FoxO1 was incubated with glutathione-Sepharose beads coated with bacterially expressed GST alone or GST-TSC2 for 6 h at 4 °C. The retained *in vitro* translated FoxO1 proteins were separated on SDS-PAGE followed by Western blotting with anti-FOXO1 antibody. The *bottom panel* shows 10% of input of GST-mutant TSC2s stained with Coomassie Blue.

fragments. Because the yeast two-hybrid screening identified the C-terminal fragment of TSC2 (amino acids 1280–1815), we constructed several deleted Tsc2 mutants in this region (Fig. 3*a*). Using *in vitro* translated wild type FoxO1, pulldown assays with GST-deleted TSC2 fusion proteins were performed and showed that FoxO1 interacted with the C-terminal TSC2 fragment (amino acids 1280–1686) directly. The FoxO1-binding site on TSC2 protein encompasses amino acids 1280–1499 (Fig. 3*b*, *lane 3*), located near the GAP domain of TSC2. These data suggest that FoxO1 binds to TSC2 directly.

FoxO1 Co-localizes with TSC2 in Cytoplasm—To examine subcellular localization of the FoxO1/TSC2 interaction, we transfected SV40-transformed hepatocytes with pCAG/FLAG-rTSC2DEE, transduced them with adenovirus encoding with HA-WT or ADA FoxO1 (30), and performed immunofluorescence using anti-TSC2 polyclonal and anti-HA monoclonal antibodies. In this cell line, even in the absence of serum, 70–80% of wild type FoxO1 was located in cytoplasm until 48 h after transduction (data not shown), where it co-localized with TSC2. In contrast, FLAG-TSC2 failed to co-localize with constitutively nuclear HA-tagged ADA FoxO1 (Fig. 4*a*). These data demonstrate that FoxO1 co-localizes with TSC2 in cytoplasm.

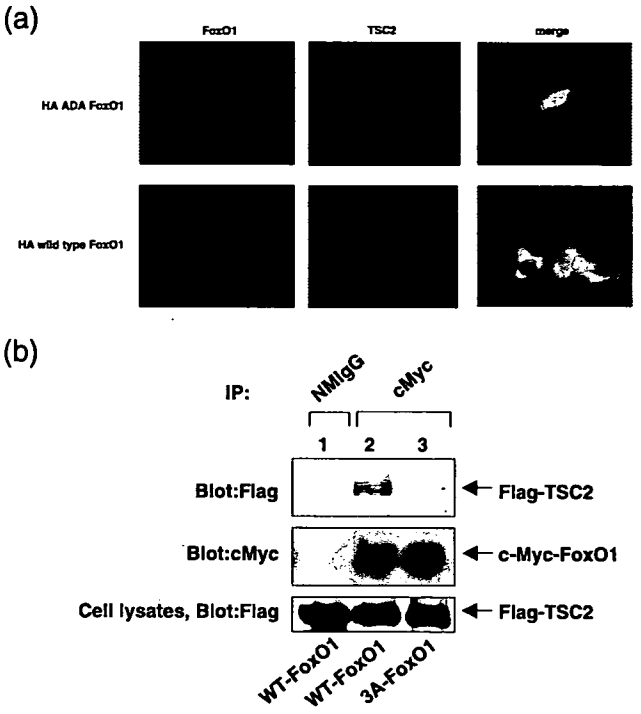

FIGURE 4. **Co-localization and co-immunoprecipitation of FoxO1 with TSC2 in cytoplasm.** *a*, FoxO1 is co-localized with TSC2 in cytoplasm and not in nucleus. SV40-transformed hepatocytes were transiently transfected with FLAG-TSC2 followed by transduction with adenovirus encoding a constitutively active HA-ADA FoxO1 (*upper panel*) or HA wild type FoxO1 (*lower panel*), and immunofluorescence was performed as described under "Experimental Procedures." *b*, constitutively active mutant FoxO1 (3A) in which three Akt phosphorylation sites (Thr-24, Ser-253, and Ser-316) were substituted to alanine residues binds to TSC2 weakly compare with wild type FoxO1. SV40-transformed hepatocytes were co-transfected with c-Myc-WT FoxO1 (*lanes 1* and *2*) or -3A FoxO1 (*lane 3*) and FLAG-TSC2 transiently. Cell lysates were immunoprecipitated (*IP*) with anti-c-Myc mouse monoclonal antibody (*lanes 2* and *3*) or normal mouse IgG (*lane 1*) and Western-blotted with anti-FLAG (*upper panel*), anti-c-Myc (*middle panel*). The *lower panel* shows Western blotting with anti-FLAG using cell lysates.

Furthermore, to examine whether FoxO1 interacts with TSC2 in cytoplasm, we used a constitutively active mutant FoxO1 (3A FoxO1) in which all three Akt phosphorylation sites were mutated to alanine (T24A/S253A/S316A; 3A FoxO1) and performed co-immunoprecipitation experiments in the same cell line. Although exogenous WT FoxO1 interacted with TSC2 as well as in HEK293 cells (Fig. 1*a*), the 3A FoxO1 interacted with TSC2 weakly compared with wild type FoxO1 (Fig. 4*b*, *lanes 2* and *3*). These data suggest the possibility that FoxO1 may associate with TSC2 in cytoplasm.

FoxO1 Inhibits TSC2 and Enhances p70 S6K Phosphorylation—TSC2 regulates cellular function mainly by their inhibitory effects on mTOR and its targets p70 S6K and 4E-BP1. It is important to elucidate whether binding of FoxO1 to TSC2 affects the activity of the mTOR/p70 S6K pathway. To investigate the effects of the FoxO1/TSC2 interaction on the mTOR pathway, we transfected SV40-transformed hepatocytes with FLAG-p70 S6K followed by transduction with adenovirus encoding HA-WT FoxO1 or -ADA FoxO1, which is localized in the nucleus and active constitutively and is immunoprecipitated with anti-FLAG monoclonal antibody and blotted with anti-phospho-p70 S6K (Thr(P)-389) antibody. After serum deprivation for 24 h, p70 S6K is dephosphorylated, and insulin increases phosphorylation of p70 S6K (Fig. 5*a*, *lanes 1* and *2* and *lanes 6* and *7*). However, even in the absence of insulin, p70 S6K was phosphorylated in a dose-dependent manner of transduced WT FoxO1 (Fig. 5, *a*, *lanes 3–5*, and *b*, *left panel*). As described above, in this cell line, even after serum deprivation for 24 h, around 70 – 80% of transduced wild type FoxO1 is located in the cytoplasm (data not shown) and is phosphorylated (Fig. 5*a*, *lanes 3–5*). These data indicate that FoxO1 is constantly phosphorylated in this cell line even in the absence of serum and insulin. In contrast, p70 S6K was dephosphorylated in cells transduced with the ADA-FoxO1 (Fig. 5, *a*, *lanes 8–10*, and *b*, *right panel*). These data suggest that FoxO1 in cytosol enhances p70 S6K phosphorylation.

To confirm whether enhanced phosphorylation of p70 S6K by FoxO1 is mediated through binding to TSC2, we overexpressed FLAG-TSC2 in SV40-transformed hepatocytes transduced with adenovirus encoding HA-WT FoxO1, and we investigated the effects on phosphorylation of p70 S6K. Overexpression of TSC2 decreased phosphorylation of p70 S6K (Fig. 5*c*, *lanes 1* and *2*). Overexpression of WT FoxO1 enhanced phosphorylation of p70 S6K (Fig. 5*c*, *lanes 1* and *3*). Even in the presence of WT FoxO1, overexpression of TSC2 decreased phosphorylation of p70 S6K (Fig. 5*c*, *lanes 3* and *4*). These data suggest that cytoplasmic FoxO1 enhances phosphorylation of p70 S6K through association with endogenous TSC2. These data also suggest the possibility that cytoplasmic FoxO1 may affect an inhibitory action of TSC2 onto mTOR and activate mTOR.

FoxO1 Functions Upstream of mTOR for Activation of p70 S6K—To investigate whether enhanced phosphorylation of p70 S6K by overexpression of WT FoxO1 is mediated through mTOR activation, we treated cells with rapamycin (25 nM) and examined effects on p70 S6K phosphorylation. Overexpression of WT FoxO1 enhanced phosphorylation of p70 S6K (Fig. 6, *lanes 2* and *3*). In contrast, treatment with rapamycin abolished p70 S6K phosphorylation induced by overexpression of FoxO1 (Fig. 6, *lane 4*). These data suggest that FoxO1 enhances phosphorylation of p70 S6K through activation of mTOR and mTOR functions downstream of FoxO1 for p70 S6K phosphorylation.

FoxO1 Reduces the Association between TSC1 and TSC2—Dimerization of TSC2 with TSC1 is important for functional inhibition on the mTOR/p70 S6K pathway. To elucidate the mechanism of how FoxO1 inhibits TSC2, we transduced HUVEC with adenovirus encoding WT FoxO1 and immunoprecipitated cell lysates with anti-TSC2 (Fig. 7*a*, *lanes 3–5*), anti-TSC1 (Fig. 7*a*, *lanes 8–10*), or anti-HA antibody (Fig. 7*a*, *lanes 13–15*) and immunoblotted with anti-TSC1, anti-TSC2, or anti-HA antibody. Overexpression of WT FoxO1 increased association with TSC2 (Fig. 7*a*, *lanes 3–5*, *bottom panel*). Co-immunoprecipitation of TSC2 and TSC1 was decreased in a dose-dependent manner of transduced FoxO1 (Fig. 7*a*, *lanes 3–5* and *lanes 8–10*, *top panel*). TSC1 does not show any physical association with transduced FoxO1 (Fig. 7*a*, *lanes 8–10*, *bottom panel*, and *lanes 13–15*, *bottom panel*). Furthermore, immunoblotting with anti-TSC2 antibody (C-20), which recognizes the C terminus of TSC2, detected a short fragment of

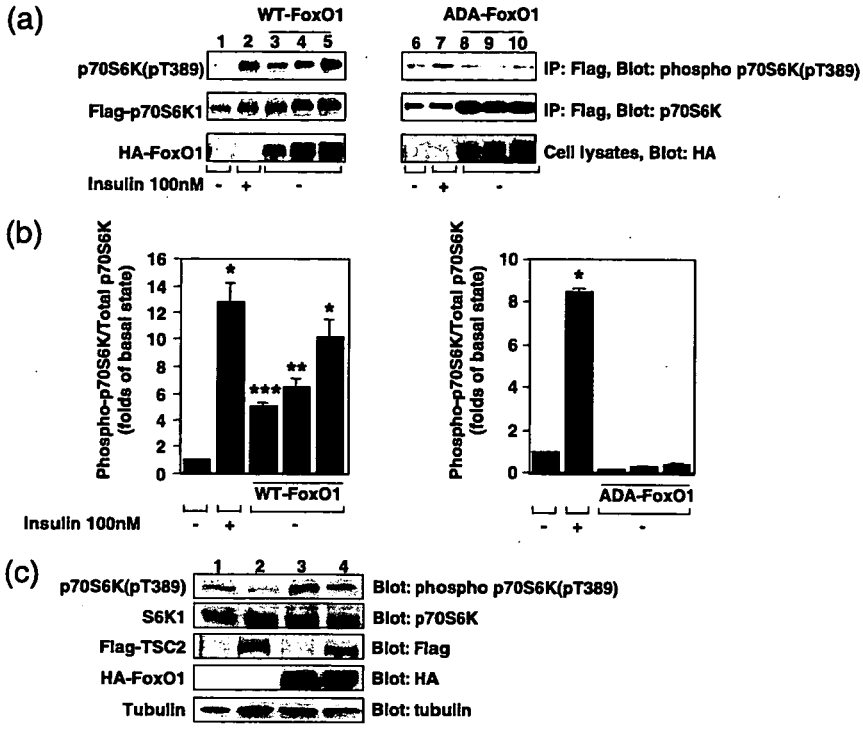

FIGURE 5. **TSC2 inhibits enhanced phosphorylation of p70 S6K induced by overexpression of WT FoxO1.** *a*, SV40-transformed hepatocytes were transfected with FLAG-p70 S6K transiently followed by transduction with adenovirus encoding HA-WT (*lanes 3–5*) or HA-ADA FoxO1 (*lanes 8–10*). At 24 h after transfection, serum deprivation was performed for 16 h, and cells were stimulated with (*lanes 2* and *7*) or without insulin (100 nM) for 30 min. Cell lysates were immunoprecipitated (*IP*) with anti-FLAG monoclonal antibody and blotted with anti-phospho-p70 S6K (pT389) (*upper panel*) or anti-p70 S6K antibody (*middle panel*). The *lower panel* shows Western blotting of transduced FoxO1 using anti-HA monoclonal antibody. *b*, ratio of phospho-p70 S6K to total p70 S6K was calculated by measuring density of bands blotted with anti-phospho-p70 S6K or total p70 S6K using NIH Image 1.62. Data were shown as folds of basal level of phospho-p70 S6K in nontransduced cells in the absence of insulin and represent mean ± S.E. from three independent experiments. *Asterisks* indicate statistically significant differences compared with the basal state (*, $p < 0.005$; **, $p < 0.02$; ***, $p < 0.05$ by one-factor ANOVA). *c*, SV40-transformed hepatocytes were transfected transiently with (*lanes 2* and *4*) or without pCAG/FLAG-TSC2 (*lanes 1* and *3*) and followed by transduction with adenovirus encoding WT FoxO1 (*lanes 3* and *4*). Cells were harvested and lysed at 48 h after transduction. Cell lysates were immunoblotted with the indicated antibodies.

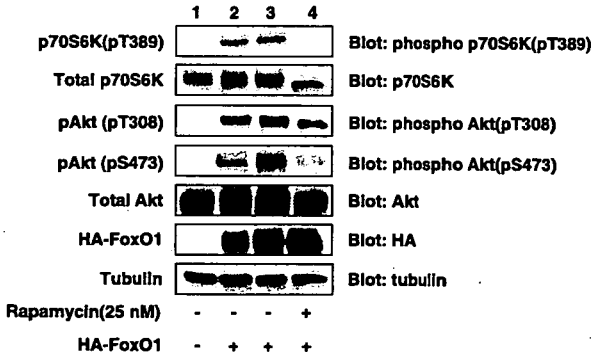

FIGURE 6. **FoxO1 enhances p70 S6K phosphorylation in a rapamycin-sensitive manner.** SV40-transformed hepatocytes were transduced with HA-WT FoxO1. At 24 h after transduction, cells were stimulated with (*lane 4*) or without (*lanes 1–3*) rapamycin (25 nM) for 24 h and harvested. Cell lysates were immunoblotted with the indicated antibodies.

TSC2, which was immunoprecipitated with FoxO1 (Fig. 7*a*, *lanes 14–15, top panel*). This short fragment of TSC2 was also detected in SV40-transformed hepatocytes (data not shown). In another set of experiments in HUVEC, WT FoxO1 decreased total amounts of full-length TSC2, which was detected by both C-20 (Fig. 7*b*, *top panel*) and N-19, which recognized the N terminus of TSC2 (Fig. 7*b*, *2nd panels*). Furthermore, the amount of short band of TSC2 was increased in a dose-dependent manner of transduced WT FoxO1 (Fig. 7*b*, *top panel*). However, we could not detect the fragmented N terminus of TSC2 by immunoblotting with N-19 antibody. These data indicate that WT FoxO1 interacts with TSC2 through its C-terminal domain, fragmented TSC2, and disrupts heterodimeric complex between TSC1 and TSC2.

Physical Association of FoxO1 with TSC2 Inhibits GAP Activity toward Rheb—From this study, FoxO1 binds to amino acids 1280–1499 of TSC2, which is near the GAP domain of TSC2. Therefore, it is possible to speculate that binding of FoxO1 may inhibit the GAP activity of TSC2. To investigate whether FoxO1 inhibits the GAP activity of TSC2 toward Rheb, we transfected cells with pCAG/FLAG-rTSC2DEE and pCA-EGFP-Rheb transiently followed by transduction with adenovirus encoding WT FoxO1 in SV40-transformed hepatocytes, and we examined guanyl nucleotide binding by EGFP-Rheb. Overexpression of TSC2 decreased %GTP by 33% compared with non-transfected cells (Fig. 8, *a*, *lanes 1* and *2*, and *b*). In contrast, overexpression of both TSC2 and FoxO1 increased %GTP by 30% compared with TSC2-transfected cells (Fig. 8*a*, *lanes 2* and *3*, and *b*). These data suggest that FoxO1 inhibits the GAP activity of TSC2 toward Rheb.

Knockdown of FOXO1 Reduces Phosphorylation of p70 S6K in HUVEC—If endogenous FoxO1 binds to TSC2 and inhibits its function, decreased expression of FoxO1 activates TSC2 and inhibits mTOR-p70 S6K pathway. To investigate whether endogenous FoxO1 inhibits TSC2, we transfected HUVEC with siRNA of FOXO1. In this cell line, both endogenous FOXO1 and TSC2 are expressed abundantly (Fig. 9 and data not shown). Knockdown of FOXO1 in HUVEC decreased FOXO1 protein level by 90% (Fig. 9, *a*, *top panel*, and *b*). Knockdown of FOXO1 inhibited phosphorylation of p70 S6K (Fig. 9, *2nd panel*). These data suggest that endogenous FOXO1 inhibits TSC2 and regulates phosphorylation of p70 S6K *in vivo*.

Prolonged Overexpression of FoxO1 Enhances Phosphorylation of Ser-307 of IRS-1—It has been reported that p70 S6K might be implicated in a negative feedback loop to suppress insulin signaling (27). From this study, we demonstrated that

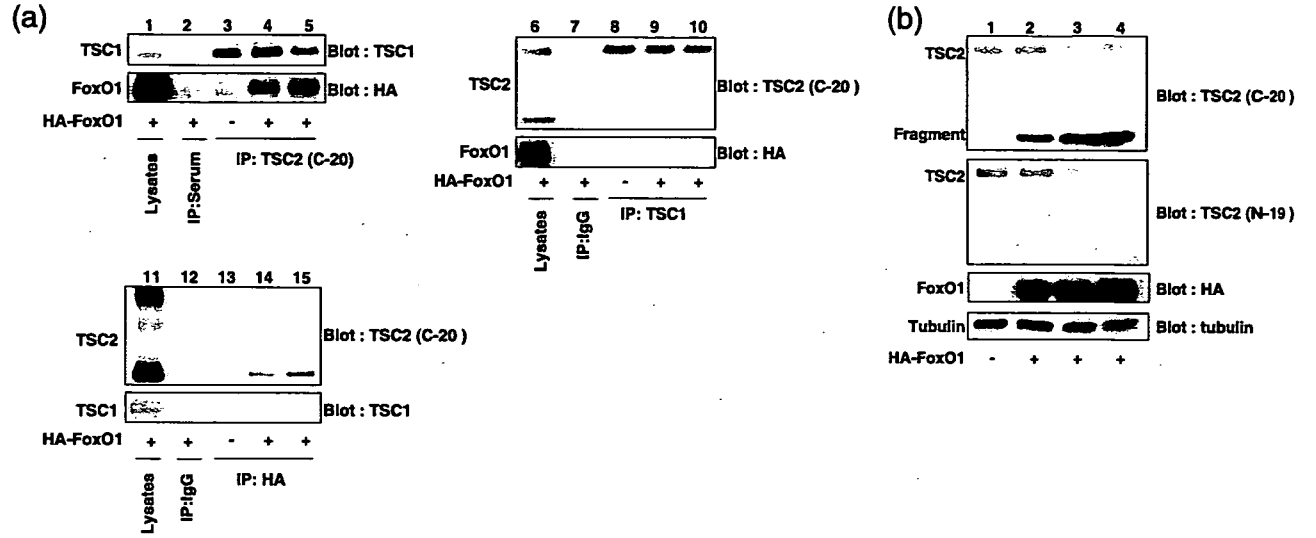

FIGURE 7. **FoxO1 reduces the association between TSC1 and TSC2.** *a*, HUVEC were transduced with adenovirus encoding HA-WT FoxO1 and were harvested 48 h later. Cell lysates were immunoprecipitated (*IP*) with normal rabbit serum (*lane 2*), normal mouse IgG (*lanes 7* and *12*), anti-TSC2 (*lanes 3–5*), anti-TSC1 (*lanes 8–10*), or anti-HA (*lanes 13–15*) and immunoblotted with the indicated antibodies. *Lanes 1, 6,* and *11* indicate cell lysates immunoblotted with the indicated antibodies. *b*, HUVEC were transduced with adenovirus encoding HA-WT FoxO1 (*lanes 2–4*) in a dose-dependent manner. At 48 h after transduction, cells were harvested and lysed. Lysates were immunoblotted with the indicated antibodies.

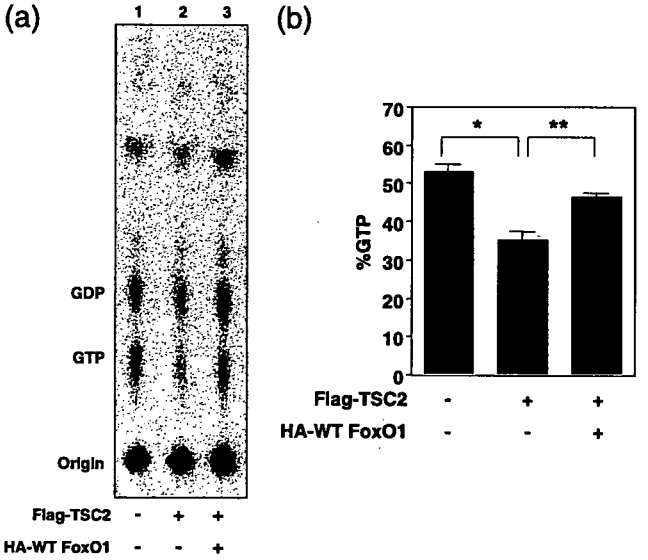

FIGURE 8. **FoxO1 inhibits GAP activity of TSC2 toward Rheb.** *a*, EGFP-Rheb in SV40-transformed hepatocytes labeled with [^{32}P]orthophosphate was immunoprecipitated with anti-GFP antibody, and the ratio of GTP to GDP bound Rheb was determined by PhosphorImager analysis following one-dimensional thin layer chromatography. Representative experiment was shown. *b*, the values of %GTP were data from three independent experiments and were shown as mean ± S.E. A *single asterisk* indicates a statistically significant difference between nontransfected and cells transfected with pCAG/FLAG-rTSC2DEE ($p < 0.001$ by one-factor ANOVA). A *double asterisk* indicates a statistically significant difference between cells transfected with pCAG/FLAG-rTSC2DEE and with both pCAG/FLAG-rTSC2DEE and WT FoxO1 ($p < 0.005$ by one-factor ANOVA).

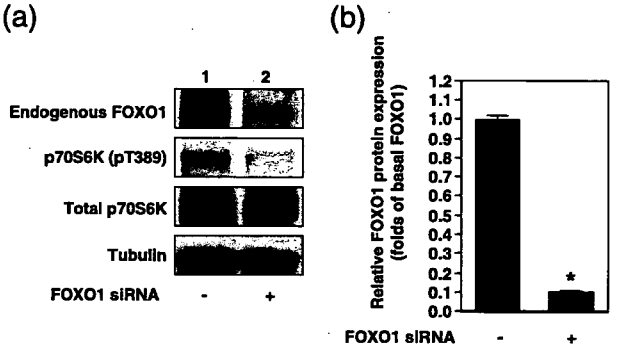

FIGURE 9. **Knockdown of endogenous FOXO1 reduces phosphorylation of p70 S6K in HUVEC.** *a*, HUVEC were transfected as described under "Experimental Procedures." At 48 h after transfection, cells were harvested and lysed. Cell lysates were immunoblotted with the indicated antibodies. *b*, efficiency of knockdown was calculated by measuring density of bands blotted with anti-FOXO1 using NIH Image 1.62. Data were shown as folds of FOXO1 protein expression in nontransfected cells and represent mean ± S.E. from three independent experiments. A *single asterisk* indicates a statistically significant difference ($p < 0.001$ by one-factor ANOVA).

cytosolic FoxO1 bound to and inhibited TSC2 and enhanced phosphorylation of p70 S6K. We speculate that enhanced phosphorylation of p70 S6K may lead to phosphorylation of serine 307 in IRS-1, which is one of the phosphorylation sites by p70 S6K (39), and finally to decreased phosphorylation of Akt and FoxO1 itself. To investigate whether FoxO1-TSC2 binding affects phosphorylation of serine 307 of IRS1 or not, we transduced SV40-transformed hepatocytes with adenoviruses encoding LacZ or WT FoxO1 and cultured cells in the presence of serum, and we examined phosphorylation of serine 307 of IRS-1 in a time course study. Phosphorylation of p70 S6K in WT FoxO1-transduced cells at 48 and 72 h is increased compared with LacZ-transduced cells because of inhibition of TSC2 by overexpression of FoxO1 from the previous experiments (Fig. 10*a*, *3rd top panel*). Amounts of total IRS1 protein level showed no significant differences between LacZ- and WT FoxO1-transduced cells (Fig. 10*a*, *lanes 1–6, 2nd top panel*). However, phosphorylation of serine 307 of IRS1 in WT FoxO1-transduced cells is increased significantly compared with LacZ-transduced cells at 72 h after transduction (Fig. 10, *a*, *lanes 3* and *6*, *top panel*, and *b*). Furthermore, at 72 h after transduction, phosphorylation of both threonine 308 and serine 473 of

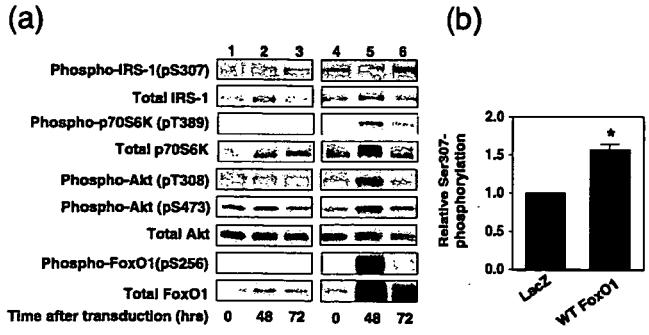

FIGURE 10. **Prolonged overexpression of wild type FoxO1 enhances phosphorylation of serine 307 of IRS1.** *a*, SV40-transformed hepatocytes were transduced with adenovirus encoding LacZ (*lanes 2* and *3*) or HA wild type FoxO1 (*lanes 5* and *6*) and cultured with complete medium at the indicated time. Culture medium was exchanged every day. Cell lysates were electrophoresed in SDS-PAGE and blotted with the indicated antibodies. *b*, intensity of bands blotted with anti-phospho-IRS1 (*pS307*) at 72 h after transduction were measured using NIH Image 1.62. Data represent mean ± S.E. from three independent experiments. An *asterisk* indicates a statistically significant difference ($p < 0.005$ by one-factor ANOVA).

Akt was decreased even in the presence of serum and also phosphorylation of FoxO1 itself was decreased. These data suggest that FoxO1-TSC2 binding leads to enhanced phosphorylation of serine 307 of IRS-1 protein through increased phosphorylation of p70 S6K and finally inhibits phosphorylation of Akt and FoxO1 itself even in the presence of serum.

DISCUSSION

In this study, we identified TSC2 as a novel FoxO1-binding protein by a yeast two-hybrid screening using a murine islet cDNA library. FoxOs interact with several kinds of protein and regulate their function and vice versa. For example, FoxO1 binds to the transcriptional co-activator PGC-1α, and PGC-1α potentiates FoxO1-dependent transcription of gluconeogenic genes (40). Acetylation by Cbp/P300 and deacetylation by Sirt1 regulates transcriptional activity of FoxOs (6). Therefore, it is important for understanding the mechanism of how FoxO1 is regulated to identify FoxO1-binding proteins. However, there are few reports about the identification of FoxO1-binding proteins using comprehensive strategies.

We used a murine islet cDNA library for identification of FoxO1-binding proteins because FoxO1 is expressed in pancreatic β-cells abundantly and has been reported already to play an important role for compensatory hypertrophy of β-cells under insulin resistance (41–43). Therefore, we speculated that it might be easy to identify FoxO1-binding proteins by using an islet cDNA library.

One of interesting findings in this study is that only FoxO1 binds to TSC2 among FoxOs. We used a fragment (amino acids 424–550) of the C terminus of FoxO1 as bait for a yeast two-hybrid screening. Amino acid sequences in this region of FoxO1, except the LXXLL motif (amino acids 459–463) (44), have low similarity among FoxOs. Therefore, it is reasonable for only FoxO1 to associate with TSC2 physically. These findings suggest the hypothesis that FoxO1 may have specific roles *in vivo*. Studies using genetically modified mice, such as knockout and transgenic mice, support this hypothesis. FoxO1-null mice die at embryonic day 10.5 from defects in angiogenesis (45). Heterozygous mutant mice of FoxO1 are viable and rescue phenotype in heterozygous knock-out mice of insulin receptor or high fat diet-induced mice (46, 47). FoxO3a-null mice are viable, and their main defect is an age-dependent female infertility because of premature activation of ovarian follicles (45, 48). FoxO4-null mice are also viable and do not show any overt phenotype (45). Each FoxO family member may have a different function *in vivo* because of distinct patterns or different regulations of each protein.

Several studies in *Drosophila* demonstrated that TSC2 forms complex with TSC1, and this complex is important for cell growth regulation (13, 49–51). This complex is assembled with rapid kinetics post-translationally serving to stabilize TSC1 and TSC2, which are ubiquitylated and degraded in their monomeric forms (18, 52, 53). TSC2 interacts with TSC1 through the N-terminal region and appears to function as a heterodimer (49, 50, 51). We demonstrated that FoxO1 bound to the C-terminal domain (amino acids 1280–1499) of TSC2, and thereafter TSC2 was fragmented when FoxO1 was overexpressed in HUVEC as shown in Fig. 7*a*. This C-terminal fragment of TSC2 was still bound to FoxO1. However, TSC1 could not bind to this C-terminal fragment of TSC2 any more because TSC1 bound to the N terminus of TSC2. After these events, the association between TSC1 and TSC2 was reduced to negatively regulate its function. The C terminus of TSC2 has a GAP domain (amino acids 1517–1674) (54). It has been demonstrated that TSC2 functions as a GAP toward Rheb, which is a small G protein implicated genetically as a positive regulator of mTOR (55–58), and that TSC2 represses Rheb function (59–62). This study demonstrated that FoxO1 binds to an adjacent region near the GAP domain of TSC2 directly and inhibits the GAP activity toward Rheb. Inhibition of TSC2 by FoxO1 leads to enhanced phosphorylation of p70 S6K. In contrast, we demonstrated that knockdown of endogenous FOXO1 by around 90% decreased phosphorylation of p70 S6K in HUVEC. These data indicate that endogenous FOXO1 has an important role for regulation of phosphorylation of p70 S6K and might suggest a novel cross-talk between Akt/FoxO1 and mTOR/p70 S6K pathway through TSC2.

It has been reported that p70 S6K may be implicated in a negative feedback loop to suppress insulin signaling. High fat-dieted *p70 S6K1*$^{-/-}$ mice remained insulin-sensitive, and knockdown of p70 S6K1 also potentiates insulin-induced Akt phosphorylation (39). p70 S6K has an inhibitory effect on Akt activation downstream of insulin receptor. p70 S6K enhances IRS-1 serine phosphorylation, which leads to decreased Akt phosphorylation and causes insulin resistance (39). It has been suggested that p70 S6K mediates IRS-1 serine phosphorylation, disrupting its interaction with IR and leading to its degradation (63). Furthermore, degradation of phosphorylated IRS-1 is mediated by its association with a 14-3-3 family member, which relocates IRS-1 from low density microsomes to the cytosol, where it can be accessed and degraded by the 26 S proteasome (64). In this study, overexpression of WT FoxO1 in SV40-transformed hepatocytes enhanced phosphorylation of serine 307 of IRS-1 and decreased Akt phosphorylation at 72 h after transduction. In concordance with this result, phosphorylation of p70 S6K was enhanced. Finally, phosphorylation of WT FoxO1

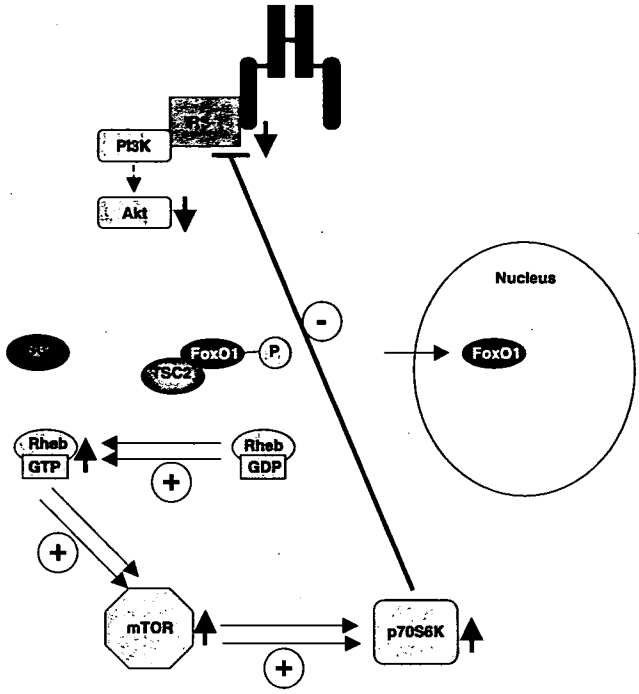

FIGURE 11. **Model depicting effects of interaction between FoxO1 and TSC2 on mTOR/p70 S6K/IRS-1 pathway.** FoxO1 in cytosol binds to TSC2 and dissociates the TSC1-TSC2 complex and inhibits the GAP activity toward Rheb. These events lead to activation of Rheb/mTOR/p70 S6K. Finally, IRS-1/PI3K/Akt pathway is inhibited through a negative feedback. After inactivation of IRS-1/PI3K/Akt pathway, FoxO1 is dephosphorylated and entered into nucleus and activates its target gene expression. A *plus* indicates an active effect, and a *minus* indicates an inhibitory effect.

itself was blunted even in the presence of serum. These data suggest a novel mechanism in which FoxO1 in cytosol can regulate Akt/FoxO1 through the TSC2/mTOR/p70 S6K/IRS1 pathway (Fig. 11).

In conclusion, these studies identified TSC2 as a novel interacting protein with FoxO1 and suggested that FoxO1 could negatively regulate TSC2 function. They suggest a novel cross-talk between Akt/FoxO1 and the mTOR/p70 S6K pathway and propose the possibility that FoxO1 can induce insulin resistance not only through increased gene expression in the nucleus but also through down-regulation insulin signaling in the cytosol. Therefore, regulation of the association between FoxO1 and TSC2 should be a target of therapy of type 2 diabetes.

Acknowledgments—We thank Susumu Seino (Division of Cellular and Molecular Medicine, Kobe University Graduate School of Medicine) for supplying the murine islet cDNA library and kindly making available the laboratory to accomplish this work. We also thank Kenta Hara (Department of Geriatric Medicine, Kobe University Graduate School of Medicine) and Kazuyoshi Yonezawa (Biosignal Research Center, Kobe University) for supplying the pMT2/FLAG-p70 S6K vector.

REFERENCES

1. Ogg, S., Paradis, S., Gottlieb, S., Patterson, G. I., Lee, L., Tissenbaum, H. A., and Ruvkun, G. (1997) *Nature* **389,** 994–999
2. Lin, K., Dorman, J. B., Rodan, A., and Kenyon, C. (1997) *Science* **278,** 1319–1322
3. Lin, K., Hsin, H., Libina, N., and Kenyon, C. (2001) *Nat. Genet.* **28,** 139–145
4. Stocker, H., and Hafen, E. (2000) *Curr. Opin. Genet. Dev.* **10,** 529–535
5. Puig, O., Marr, M. T., Ruhf, M. L., and Tjian, R. (2003) *Genes Dev.* **17,** 2006–2020
6. Accili, D., and Arden, K. C. (2004) *Cell* **117,** 421–426
7. Furuyama, T., Nakazawa, T., Nakano, I., and Mori, N. (2000) *Biochem. J.* **349,** 629–634
8. Greer, E. L., and Brunet, A. (2005) *Oncogene* **24,** 7410–7425
9. Fingar, D. C., and Blenis, J. (2004) *Oncogene* **23,** 3151–3171
10. The European Chromosome 16 Tuberous Sclerosis Consortium (1993) *Cell* **75,** 1305–1315
11. Hay, N., and Sonenberg, N. (2004) *Genes Dev.* **18,** 1926–1945
12. Sparagana, S. P., and Roach, E. S. (2000) *Curr. Opin. Neurol.* **13,** 115–119
13. Ito, N., and Rubin, G. M. (1999) *Cell* **96,** 529–539
14. Gao, X., Zhang, Y., Arrazola, P., Hino, O., Kobayashi, T., Yeung, R. S., Ru, B., and Pan, D. (2002) *Nat. Cell Biol.* **4,** 699–704
15. Goncharova, E. A., Goncharov, D. A., Eszterhas, A., Hunter, D. S., Glassberg, M. K., Yeung, R. S., Walker, C. L., Noonan, D., Kwiatkowski, D. J., Chou, M. M., Panettieri, R. A., Jr., and Krymskaya, V. P. (2002) *J. Biol. Chem.* **277,** 30958–30967
16. Kwiatkowski, D. J., Zhang, H., Bandura, J. L., Heiberger, K. M., Glogauer, M., el-Hashemite, N., and Onda, H. (2002) *Hum. Mol. Genet.* **11,** 525–534
17. Tee, A. R., Fingar, D. C., Manning, B. D., Kwiatkowski, D. J., Cantley, L. C., and Blenis, J. (2002) *Proc. Natl. Acad. Sci. U. S. A.* **99,** 13571–13576
18. Inoki, K., Li, Y., Zhu, T., Wu, J., and Guan, K. L. (2002) *Nat. Cell Biol.* **4,** 648–657
19. Manning, B. D., Tee, A. R., Logsdon, M. N., Blenis, J., and Cantley, L. C. (2002) *Mol. Cell* **10,** 151–162
20. Potter, C. J., Pedraza, L. G., and Xu, T. (2002) *Nat. Cell Biol.* **4,** 658–665
21. Manning, B. D., and Cantley, L. C. (2003) *Trends Biochem. Sci.* **28,** 573–576
22. Li, Y., Corradetti, M. N., Inoki, K., and Guan, K. L. (2004) *Trends Biochem. Sci.* **29,** 32–38
23. Corradetti, M. N., Inoki, K., Bardeesy, N., DePinho, R. A., and Guan, K. L. (2004) *Genes Dev.* **18,** 1533–1538
24. Inoki, K., Zhu, T., and Guan, K. L. (2003) *Cell* **115,** 577–590
25. Shaw, R. J., Bardeesy, N., Manning, B. D., Lopez, L., Kosmatka, M., DePinho, R. A., and Cantley, L. C. (2004) *Cancer Cell* **6,** 91–99
26. Sofer, A., Lei, K., Johannessen, C. M., and Ellisen, L. W. (2005) *Mol. Cell. Biol.* **25,** 5834–5845
27. Um, S. H., D'Alessio, D., and Thomas, G. (2006) *Cell Metab.* **3,** 393–402
28. Hara, K., Yonezawa, K., Kozlowski, M. T., Sugimoto, T., Andrabi, K., Weng, Q. P., Kasuga, M., Nishimoto, I., and Avruch, J. (1997) *J. Biol. Chem.* **272,** 26457–26463
29. Nakae, J., Park, B. C., and Accili, D. (1999) *J. Biol. Chem.* **274,** 15982–15985
30. Nakae, J., Kitamura, T., Silver, D. L., and Accili, D. (2001) *J. Clin. Investig.* **108,** 1359–1367
31. Takaishi, H., Konishi, H., Matsuzaki, H., Ono, Y., Shirai, Y., Saito, N., Kitamura, T., Ogawa, W., Kasuga, M., Kikkawa, U., and Nishizuka, Y. (1999) *Proc. Natl. Acad. Sci. U. S. A.* **96,** 11836–11841
32. Kamioka, Y., Fukuhara, S., Sawa, H., Nagashima, K., Masuda, M., Matsuda, M., and Mochizuki, N. (2004) *J. Biol. Chem.* **279,** 40091–40099
33. Tsuchiya, H., Orimoto, K., Kobayashi, K., and Hino, O. (1996) *Cancer Res.* **56,** 429–433
34. Niwa, H., Yamamura, K., and Miyazaki, J. (1991) *Gene (Amst.)* **108,** 193–199
35. Nakae, J., Barr, V., and Accili, D. (2000) *EMBO J.* **19,** 989–996
36. Nishimura, M., Yokoi, N., Miki, T., Horikawa, Y., Yoshioka, H., Takeda, J., Ohara, O., and Seino, S. (2004) *DNA Res.* **11,** 315–323
37. Klein, J., Fasshauer, M., Ito, M., Lowell, B. B., Benito, M., and Kahn, C. R. (1999) *J. Biol. Chem.* **274,** 34795–34802
38. Nabekura, T., Otsu, M., Nagasawa, T., Nakauchi, H., and Onodera, M. (2006) *Mol. Ther.* **13,** 301–309
39. Um, S. H., Frigerio, F., Watanabe, M., Picard, F., Joaquin, M., Sticker, M., Fumagalli, S., Allegrini, P. R., Kozma, S. C., Auwerx, J., and Thomas, G. (2004) *Nature* **431,** 200–205

40. Puigserver, P., Rhee, J., Donovan, J., Walkey, C. J., Yoon, J. C., Oriente, F., Kitamura, Y., Altomonte, J., Dong, H., Accili, D., and Spiegelman, B. M. (2003) *Nature* **423,** 550–555
41. Kitamura, T., Nakae, J., Kitamura, Y., Kido, Y., Biggs, W. H., III, Wright, C. V., White, M. F., Arden, K. C., and Accili, D. (2002) *J. Clin. Investig.* **110,** 1839–1847
42. Kitamura, Y. I., Kitamura, T., Kruse, J. P., Raum, J. C., Stein, R., Gu, W., and Accili, D. (2005) *Cell Metab.* **2,** 153–163
43. Okamoto, H., Hribal, M. L., Lin, H. V., Bennett, W. R., Ward, A., and Accili, D. (2006) *J. Clin. Investig.* **116,** 775–782
44. Nakae, J., Cao, Y., Daitoku, H., Fukamizu, A., Ogawa, W., Yano, Y., and Hayashi, Y. (2006) *J. Clin. Investig.* **116,** 2473–2483
45. Hosaka, T., Biggs, W. H., III, Tieu, D., Boyer, A. D., Varki, N. M., Cavenee, W. K., and Arden, K. C. (2004) *Proc. Natl. Acad. Sci. U. S. A.* **101,** 2975–2980
46. Nakae, J., Biggs, W. H., Kitamura, T., Cavenee, W. K., Wright, C. V., Arden, K. C., and Accili, D. (2002) *Nat. Genet.* **32,** 245–253
47. Nakae, J., Kitamura, T., Kitamura, Y., Biggs, W. H., III, Arden, K. C., and Accili, D. (2003) *Dev. Cell* **4,** 119–129
48. Castrillon, D. H., Miao, L., Kollipara, R., Horner, J. W., and DePinho, R. A. (2003) *Science* **301,** 215–218
49. Potter, C. J., Huang, H., and Xu, T. (2001) *Cell* **105,** 357–368
50. Gao, X., and Pan, D. (2001) *Genes Dev.* **15,** 1383–1392
51. Tapon, N., Ito, N., Dickson, B. J., Treisman, J. E., and Hariharan, I. K. (2001) *Cell* **105,** 345–355
52. Nellist, M., van Slegtenhorst, M. A., Goedbloed, M., van den Ouweland, A. M., Halley, D. J., and van der Sluijs, P. (1999) *J. Biol. Chem.* **274,** 35647–35652
53. Benvenuto, G., Li, S., Brown, S. J., Braverman, R., Vass, W. C., Cheadle, J. P., Halley, D. J., Sampson, J. R., Wienecke, R., and DeClue, J. E. (2000) *Oncogene* **19,** 6306–6316
54. Li, Y., Inoki, K., and Guan, K. L. (2004) *Mol. Cell. Biol.* **24,** 7965–7975
55. Wienecke, R., Konig, A., and DeClue, J. E. (1995) *J. Biol. Chem.* **270,** 16409–16414
56. Xiao, G. H., Shoarinejad, F., Jin, F., Golemis, E. A., and Yeung, R. S. (1997) *J. Biol. Chem.* **272,** 6097–6100
57. Garami, A., Zwartkruis, F. J., Nobukuni, T., Joaquin, M., Roccio, M., Stocker, H., Kozma, S. C., Hafen, E., Bos, J. L., and Thomas, G. (2003) *Mol. Cell* **11,** 1457–1466
58. Tee, A. R., Manning, B. D., Roux, P. P., Cantley, L. C., and Blenis, J. (2003) *Curr. Biol.* **13,** 1259–1268
59. Inoki, K., Li, Y., Xu, T., and Guan, K. L. (2003) *Genes Dev.* **17,** 1829–1834
60. Zhang, Y., Gao, X., Saucedo, L. J., Ru, B., Edgar, B. A., and Pan, D. (2003) *Nat. Cell Biol.* **5,** 578–581
61. Stocker, H., Radimerski, T., Schindelholz, B., Wittwer, F., Belawat, P., Daram, P., Breuer, S., Thomas, G., and Hafen, E. (2003) *Nat. Cell Biol.* **5,** 559–565
62. Saucedo, L. J., Gao, X., Chiarelli, D. A., Li, L., Pan, D., and Edgar, B. A. (2003) *Nat. Cell Biol.* **5,** 566–571
63. Harrington, L. S., Findlay, G. M., Gray, A., Tolkacheva, T., Wigfield, S., Rebholz, H., Barnett, J., Leslie, N. R., Cheng, S., Shepherd, P. R., Gout, I., Downes, C. P., and Lamb, R. F. (2004) *J. Cell Biol.* **166,** 213–223
64. Craparo, A., Freund, R., and Gustafson, T. A. (1997) *J. Biol. Chem.* **272,** 11663–11669

Available online at www.sciencedirect.com
SCIENCE DIRECT
Cellular Signalling 18 (2006) 994–1005
CELLULAR SIGNALLING
www.elsevier.com/locate/cellsig

ERK is an anti-inflammatory signal that suppresses expression of NF-κB-dependent inflammatory genes by inhibiting IKK activity in endothelial cells

Yong-Sun Maeng [a,1], Jeong-Ki Min [a,1], Jeong Hun Kim [b], Akiko Yamagishi [c], Naoki Mochizuki [c], Ja-Young Kwon [d], Yong-Won Park [d], Young-Myeong Kim [e], Young-Guen Kwon [a,*]

[a] *Department of Biochemistry College of Sciences, Yonsei University, Seoul 120-749, Korea*
[b] *Department of Ophthalmology Seoul National University College of Medicine, Seoul Artificial Eye Center, Clinical Research Institute, Seoul National University Hospital, Seoul 110-744, Korea*
[c] *Department of Structural Analysis, National Cardiovascular Center Research Institute, 5-7-1 Fujishirodai, Suita, Osaka 565-8565, Japan*
[d] *Department of Obstetrics and Gynecology Yonsei University College of Medicine 134 Shinchon-dong, Seodaemoon-gu Seoul 120-752, Korea*
[e] *Department of Molecular and Cellular Biochemistry, School of Medicine, Kangwon National University, Chunchon, Kangwon-Do 200-701, Korea*

Received 29 July 2005; received in revised form 20 August 2005; accepted 22 August 2005
Available online 20 October 2005

Abstract

Unveiling of endothelial nuclear factor-κB (NF-κB) activation is pivotal for understanding the inflammatory reaction and the pathogenesis of inflammatory vascular diseases. We here report the novel function of extracellular signal-related kinase (ERK) in controlling endothelial NF-κB activation and inflammatory responses. In human endothelial cells, vascular endothelial growth factor (VEGF) induced NF-κB-dependent transcription of cell adhesion molecules (CAMs) and monocyte adhesion. These effects were prominently enhanced by either pretreatment with the MEK inhibitors, PD98059 and U0126 or overexpression of a dominant negative form of MEK, but blocked by a wild type ERK. Consistently, inhibition of ERK significantly increased IκB kinase (IKK) activity, IκBα phosphorylation, and nuclear translocation of NF-κB induced by VEGF, whereas overexpression of ERK resulted in the loss of these responses to VEGF. Using two PKC inhibitors has demonstrated that VEGF concomitantly stimulates IKK and its negative regulatory signal ERK through PKC that lies downstream of KDR/Flk-1. Strikingly, elevation of ERK in endothelial cells markedly inhibited CAM expression and NF-κB activation as well as monocyte adhesion induced by IL-1β and TNF-α. The data collectively suggest that ERK serves as an anti-inflammatory signal that suppresses expression of NF-κB-dependent inflammatory genes by inhibiting IKK activity in endothelial cells. Measuring the existence of ERK activity in vascular endothelial cells may be useful for predicting the feasibility and potency of inflammatory reactions in the vasculature.

Keywords: VEGF; ERK; NF-κB; CAMs; Inflammation

1. Introduction

Inflammatory conditions are characterized by the migration of proliferating leucocytes from the blood to the tissues and involve a coordinated series of adhesion processes between circulating and resident leukocytes and the vascular endothelium [1–3]. These events are controlled by different types of adhesion molecules on the leukocytes and endothelium [3]. In particular, expression of cell adhesion molecules (CAMs), such as E-selectin, intercellular adhesion molecule-1 (ICAM-1), and vascular cell adhesion molecule-1 (VCAM-1),

Abbreviations: VEGF, vascular endothelial growth factor; HUVECs, human umbilical vein endothelial cells; bFGF, basic fibroblast growth factor; EGF, epidermal growth factor; TNF-α, tumor necrosis factor-α; IL-1β, interleukin-1β; KDR, Flk-1/kinase-insert domain containing receptor; VCAM-1, vascular cell adhesion molecule-1; ICAM-1, intercellular adhesion molecule-1; PI3K, phosphatidylinositol 3′-kinase; PLC, phospholipase C; PKC, protein kinase C; IKK, IκB kinase; MEK, mitogen-activated protein/extracellular signal-regulated kinase kinase; ERK, extracellular signal-regulated kinase; RT-PCR, reverse transcriptase-polymerase chain reaction.

* Corresponding author. Tel.: +82 2 2123 5697; fax: +82 2 362 9897.
E-mail address: ygkwon@yonsei.ac.kr (Y.-G. Kwon).
[1] These authors contributed equally to this study.

0898-6568/$ - see front matter © 2005 Elsevier Inc. All rights reserved.
doi:10.1016/j.cellsig.2005.08.007

on the surface of endothelial cells is required for endothelial–leukocyte cell interaction [1]. In the absence of inflammation, CAM expression is low on the endothelial cells of most vascular beds, but it dramatically increases in response to a number of extracellular stimuli, including tumor necrosis factor-α (TNF-α), interleukin-1β (IL-1β), vascular endothelial growth factor (VEGF), and bacterial lipopolysaccharides [4–6]. Among the classical transcription factors activated by inflammatory cytokines, nuclear factor-κB (NF-κB) plays a pivotal role in the regulation of inflammatory response genes [7,8]. Indeed, it is considered to be a major transcriptional regulator of CAMs in endothelial cells [9].

In mammalian, the five members of the NF-κB family, p65 (RelA), RelB, c-Rel, p50/p105 (NF-κB1), and p52/p100 (NF-κB2), exist in quiescent cells as homo- or heterodimers bound to IκB family proteins and retained in the cytoplasm as an inactive state [10]. In stimulated cells, IκB is degraded through the ubiquitin-proteasome pathway upon specific phosphorylation by activated IκB kinase (IKK) [11]. The IKK activity in cells can be purified as a 700–900-kDa complex, and has been shown to contain two kinase subunits, IKKα (IKK1) and IKKβ (IKK2), and a regulatory subunit, NEMO (NF-κB essential modifier) or IKKγ [11–13]. In the canonical NF-κB signaling pathway, IKKβ is both necessary and sufficient for phosphorylation of IκBα on Ser 32 and Ser 36, and IκBβ on Ser 19 and Ser 23 [12]. By contrast, although the role of IKKα in the canonical pathway is unclear, recent studies suggest that the IKKα subunit phosphorylates p100 and causes its inducible processing to p52 [13].

The activation of the IKK complex is suggested to be exerted by phosphorylation of the IKK complex by the mitogen-activated protein kinase kinase kinase (MAP3K) family including NF-κB-inducing kinase [14], mitogen-activated protein/ERK kinase kinase 1 (MEKK) [15], MEKK3 [16], TGF-β activating kinase 1 [17] and NF-κB-activating kinase [18]. The MAP3K family phosphorylated and induced NF-κB activation when overexpressed or when assayed in vitro, but the mechanism by which cytokines lead to the activation of the IKK complex in vivo is still controversial [19]. Alternatively, previous studies have also suggested that IKK recruitment to receptor complexes at the cell membrane results in its autophosphorylation and subsequent activation [20]. Indeed, IKK recruitment to the TNF receptor-1 complex is shown to be required for TNFα-mediated activation of the IKK complex [11,21–23]. In addition, the important involvement of various intracellular adaptors such as TNF-receptor-associated factors and death-domain kinase receptor-interacting protein in receptor-mediated NF-κB pathway has been extensively reported [24]. However, despite of a large number of studies in vitro and in vivo, the specific upstream signaling mechanism that regulates the IKK activity remains for further investigation.

In the present study, we report an important regulatory role of extracellular signal-related kinase (ERK) in controlling expression of NF-κB-dependent inflammatory genes in vascular endothelial cells. We found that inhibition of ERK markedly increased CAM expression in response to VEGF, which induces both ERK and NF-κB activation in endothelial cells, and this effect was correlated with increased NF-κB activation. Furthermore, elevation of ERK activity in endothelial cells resulted in the suppression of CAM expression and NF-κB activation as well as leukocyte adhesion induced by IL-1β and TNF-α in addition to VEGF. We therefore propose that ERK is a potential intracellular regulator that suppresses vascular inflammation by inhibiting NF-κB activation in endothelial cells.

2. Materials and methods

2.1. Cell culture and reagents

Human umbilical vein endothelial cells (HUVECs) were isolated from human umbilical cord veins by collagenase treatment as described previously [25] and used in passages 2–7. The cells were grown in M199 medium (Invitrogen, Carlsbad, CA) supplemented with 20% fetal bovine serum, 100 units/ml penicillin, 100 μg/ml streptomycin, 3 ng/ml bFGF (Upstate Biotechnology, Lake Placid, NY), and 5 units/ml heparin at 37 °C in humidified 5% CO_2/95% air. U937 cells were grown in RPMI-1640 (Invitrogen). VEGF was from Upstate Biotechnology (Lake Placid, NY), PD98059 from Alexis (San Diego, CA), and U0126 and GF109203X from BIOMOL (Plymouth Meeting, PA). Chelerythrine chloride and actinomycin D were from Sigma. M199, heparin, Trizol reagent and LipofectAMINE Plus were purchased from Invitrogen. Antibodies used were as follows: rabbit anti-VCAM-1 polyclonal antibody, mouse anti-actin monoclonal antibody (Santa Cruz Biotechnology, SantaCruz, Calif), rabbit anti-phospho-IκB-α polyclonal antibody (Cell Signaling, Beverly, MA), mouse anti-phospho-ERK (Thr-202/Tyr-204) monoclonal antibody, and rabbit anti-ERK polyclonal antibody (New England Biolabs, Beverly, MA). All other reagents were purchased from Sigma unless otherwise indicated.

2.2. Construction of reporter plasmids

The VCAM-1 luciferase plasmids were constructed as described previously [26]. The human VCAM-1 promoter, spanning 1716 to +119 bp, was amplified by PCR with primers containing 5′ *KpnI* and 3′ *XhoI* restriction sites. The resulting PCR fragment was digested with *KpnI* and *XhoI* and cloned into pGL3-basic vector (Promega). Synthetic oligonucleotide sense and antisense primers were used to generate a series of DNA fragments with successive 5′ deletions. All PCR products were digested with *KpnI* and *XhoI* and cloned into pGL3-basic vector. The following deletion constructs of the human VCAM-1 promoter were generated: 1716 to +119 bp (fragment 6), 366 to +119 bp (fragment 5), 296 to +119 bp (fragment 4), 210 to +119 bp fragment 3) and 38 to +119 bp (fragment 2). To construct the ICAM-1 luciferase plasmid, we cloned regions spanning −1350 to +45 bp of the human ICAM-1 promoter into pGL3-basic vector (Promega). Plasmid DNAs were purified from bacterial cultures using an Endofree Plasmid Maxi kit (Qiagen, Chatsworth, CA). We confirmed all constructs by restriction enzyme mapping and sequencing.

2.3. Transfections and analysis of luciferase activity

HUVECs were transfected with 1 μg of the above plasmids and 1 μg of the control pCMV-β-gal plasmid using LipofectAMINE Plus reagents (Invitrogen, Carlsbad, CA). Cell extracts were prepared twenty-four hours after transfection, and luciferase assays carried out with the Luciferase Assay System (Promega). Luciferase activities were normalized with respect to parallel β-galactosidase activities, to correct for differences in transfection efficiency, and the β-galactosidase assays were performed using the β-Galactosidase Enzyme Assay System (Promega). Each experimental point was performed in at least quadruplicate.

2.4. Flow cytometry

Cells from subconfluent cultures were detached gently from plates with PBS containing 2 mM EDTA. The cells were washed two or three times with PBS, resuspended in PBS containing 3% bovine serum albumin and incubated with FITC-conjugated VCAM-1 antibody (Serotec) for 30 min on ice. They were then fixed with 2% paraformaldehyde and analyzed by flow cytometry in a fluorescence-activated cell sorter (Becton Dickinson). Each experimental condition was performed in quadruplicate.

2.5. Semi-quantitative RT-PCR analysis

Total RNA was obtained from HUVECs with a TRIzol reagent kit. 0.5–5 μg RNA samples were used in the reverse transcriptase-polymerase chain reactions (RT-PCR), and the correlation between the amounts of RNA used and quantity of PCR products from VCAM-1 mRNA and the internal standard (β-actin) mRNA was examined. Briefly, target RNA was converted to cDNA by treatment with 200 units of reverse transcriptase and 500 ng of oligo(dT) primer in 50 mM Tris–HCl (pH 8.3), 75 mM KCl, 3 mM $MgCl_2$, 10 mM dithiothreitol, and 1 mM dNTPs at 42 °C for 1 h. The reaction was stopped by heating at 70 °C for 15 min. One μl of the cDNA mixture was used for enzymatic amplification. The polymerase chain reaction was performed in 50 mM KCl, 10 mM Tris–HCl (pH 8.3), 1.5 mM $MgCl_2$, 0.2 mM dNTPs, 2.5 units of *Taq* DNA polymerase, and 0.1 μM of primers for VCAM-1. Amplification was performed in a DNA thermal cycler (model PTC-200; MJ Research) under the following condition: denaturation at 94 °C for 5 min for the first cycle and for 30 s thereafter, annealing at 60 °C (VCAM-1), for 30 s, and extension at 72 °C for 30 s for 25 repetitive cycles. Final extension was at 72 °C for 10 min. The primers used for VCAM-1 were as follows: 5′-GATACAACCGTCTTGGTCAGCCC-3′ (sense) and 5′CGC-ATCCTTCAACTGGCCTT-3′ (antisense). Each experimental condition was performed in quadruplicate.

2.6. Transfer vector constructs

HIV-vectors were produced from the previously described SIN-18 vector, which contains a large deletion in the U3 region of the 3′ long terminal repeat (LTR) [27]. The SIN.cPPT.CMV-EGFP-W vector contained the enhanced green fluorescent protein (EGFP) transgene driven by the human cytomegalovirus (CMV) immediate-early enhancer/promoter. The SIN.cPPT. ERK2-EGFP-W vector contained the human extracellular signal-related kinase 2 gene.

2.7. Lentiviral vectors and in vitro gene transfer

VSV-G-pseudotyped, HIV-1-based vector particles were produced by cotransfection of four plasmids (pMDLg/pRRE: 12 μg; pRSVrev: 3 μg; pMD.G: 5 μg, SIN vector: 20 μg) onto 293T cells. Culture medium was replaced by serum-free SFM-II medium (Invitrogen) 15 h post-transfection. Thirty-two hours later, cell supernatants were harvested, filtered through a 0.45 μm filtration system, concentrated on Centricon Plus-80 Biomax MW 100,000 (Millipore, Le-Mont-sur-Lausanne, Switzerland), resuspended in PBS, and re-concentrated on Centricon-20. The titer of the SIN.cPPT. CMV-EGFP-W vector stock solution was 5×10^9 transducing units (TU)/ml by flow cytometry on 293T cells, and 3×10^4 ng p24 antigen per ml by p24-ELISA. The SIN.cPPT.ERK2-EGFP-W vector was titered by flow cytometry on HUVECs (of note, titration of SIN.cPPT.CMV-EGFP-W yielded similar results in HUVECs and 293T cells). HUVECs were seeded in six-well plates and allowed to adhere overnight. Viral vectors were added to cell cultures at varying multiplicities of infection (MOIs ≈1–50). At 18 h, cells were washed and medium was replaced. Cells were harvested at the indicated time points. Percentages of EGFP-positive cells and their mean fluorescence values (MFVs) were determined by flow cytometry (FACScan).

2.8. Preparation of nuclear extracts and electrophoretic mobility shift assays

Cells were washed three times with ice-cold Tris-buffered saline (TBS) and resuspended in 400 μl of buffer A [10 mM HEPES (pH 7.9), 10 mM KCl, 0.1 mM EDTA, 0.1 mM EGTA, 1 mM dithiothreitol (DTT), 1 mM phenylmethylsulfonyl fluoride (PMSF), 5 μg/ml of leupeptin, and 5 μg/ml of aprotinin]. After 15 min, Nonidet P-40 (NP-40) was added to a final concentration of 0.6%. Nuclei were pelleted and suspended in 50 μl of buffer C [20 mM HEPES (pH 7.9), 0.4 M NaCl, 1 mM EDTA, 1 mM EGTA, 1 mM DTT, 1 mM PMSF, 5 μg/ml of leupeptin, and 5 μg/ml of aprotonin]. After 30 min agitation at 4 °C, the lysates were centrifuged, and the supernatants containing the nuclear proteins were diluted with buffer C. Binding reactions contained 15 μg of nuclear protein and a ^{32}P end-labeled, double-stranded oligonucleotide containing the NF-κB binding site on the human VCAM-1 promoter (5′-CCTTGAAGGGATTTCCCTCC-3′) and were incubated for 30 min. Cold competition controls were performed by preincubating the nuclear proteins with a 20-fold molar excess of unlabeled NF-κB double-stranded oligonucleotide for 20 min. The mixtures were resolved on native 5% polyacrylamide gels, which were dried and autoradiographed.

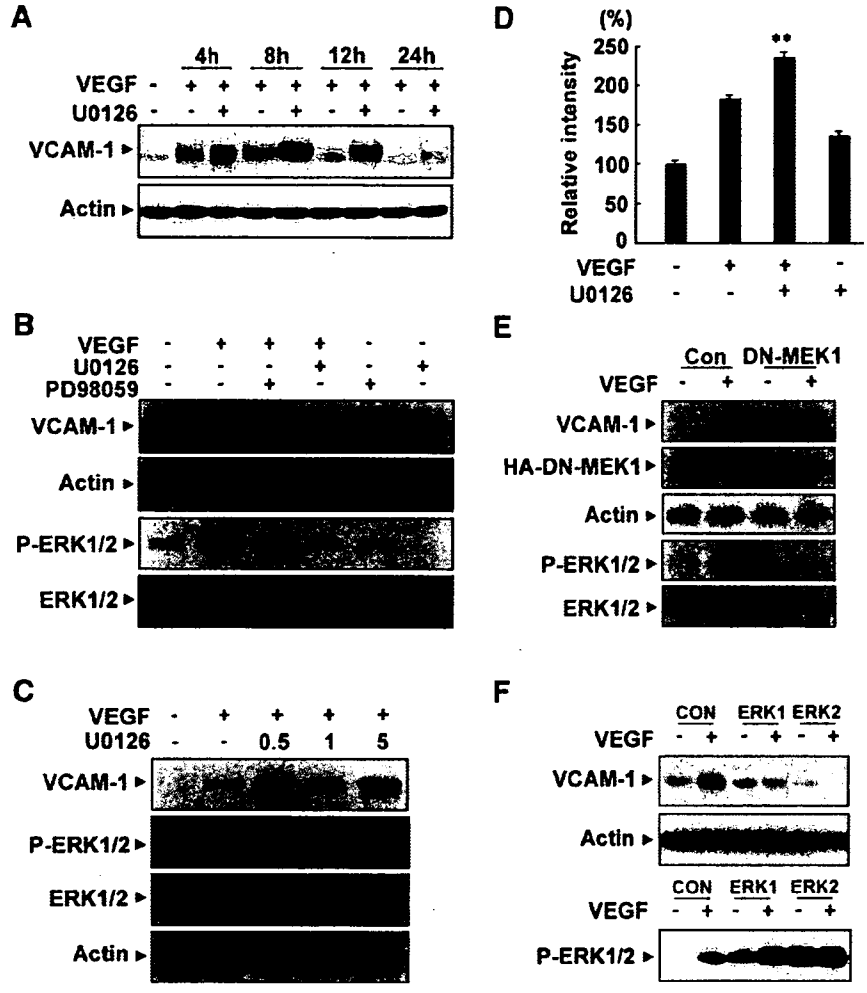

Fig. 1. Inhibition of ERK resulted in increased expression of VCAM-1 in response to VEGF. (A) HUVECs were incubated for 30 min with or without 5 μM U0126 and stimulated with 10 ng/ml VEGF for the indicated times. (B) HUVECs were pretreated for 30 min with 5 μM U0126 or 10 μM PD98059 prior to stimulation with 10 ng/ml VEGF for 10 min (*lower panel*) or 8 h (*upper panel*). (C) HUVECs were incubated for 30 min with or without various concentrations of U0126 and stimulated with 10 ng/ml VEGF for 10 min (*lower panel*) or 8 h (*upper panel*). Western blots were probed with anti-VCAM-1 antibody and an anti-phospho-ERK antibody, and reprobed with anti-actin antibody or anti-ERK antibody to verify equal loading of proteins. (D) HUVECs were pretreated for 30 min with 5 μM U0126 and then stimulated with 10 ng/ml VEGF for 8 h. The cells were detached from the plates, treated with FITC-conjugated VCAM-1 antibody and analyzed with a FACScan. Staining was quantified by flow cytometry. HUVECs were transfected with hemagglutinin (HA) tagged dominant negative form of MEK1, DN-MEK1, (E) or a wild form of ERKs (ERK1, 2) (F) and then stimulated with VEGF (10 ng/ml) for 10 min (*lower panel*) or 8 h (*upper panel*). Western blots were probed with anti-VCAM-1, anti-HA, and anti-phospho-ERK antibody and reprobed with anti-actin antibody or anti-ERK antibody to verify equal loading of proteins. Con indicates cells transfected with empty vector. **, $P<0.01$ versus VEGF alone.

Each experimental point was performed in duplicate and represents several independent conditions.

2.9. In vitro kinase assays

IKK was assayed as described previously [28]. Briefly, the IKK complex was precipitated from whole cell extracts with antibody against IKK-γ, followed by treatment with protein A-Sepharose beads (Pierce). After a 2 h incubation, the beads were washed with lysis buffer and assayed in kinase assay mixture containing 50 mM HEPES (pH 7.4), 20 mM $MgCl_2$, 2 mM dithiothreitol, 20 μCi of [γ-^{32}P]ATP, 10 μM unlabeled ATP, and 2 μg of substrate GST-IκBα (amino acids 1–54). After incubation at 30 °C for 30 min, the reaction was terminated by boiling in SDS sample buffer for 5 min. Finally, the protein was resolved on 10% SDS-PAGE, the gel was dried, and the radioactive bands were visualized with a PhosphorImager. To determine the total amounts of IKK complex in each sample, 50 μg of whole cell protein was resolved on 7.5% SDS-PAGE, electrotransferred to a nitrocellulose membrane, and blotted with anti-IKK-γ antibody. The data represent the average of two separate experiments, each performed in duplicate.

2.10. Immunocytochemical localization of p65

Nuclear translocation of the p65 subunit of NF-κB was examined by an immunocytochemical method as described previously [28]. Briefly, treated cells were fixed with 2%